ERDC TR-02-7

US Army Corps
of Engineers®
Engineer Research and
Development Center

Biaxial Loading and Failure Behavior of Brick Triplets with Fiber-Reinforced Polymer Composite Upgrades

J.B. Berman, G.K. Al-Chaar, and P.K. Dutta

December 2002

Construction Engineering
Research Laboratory

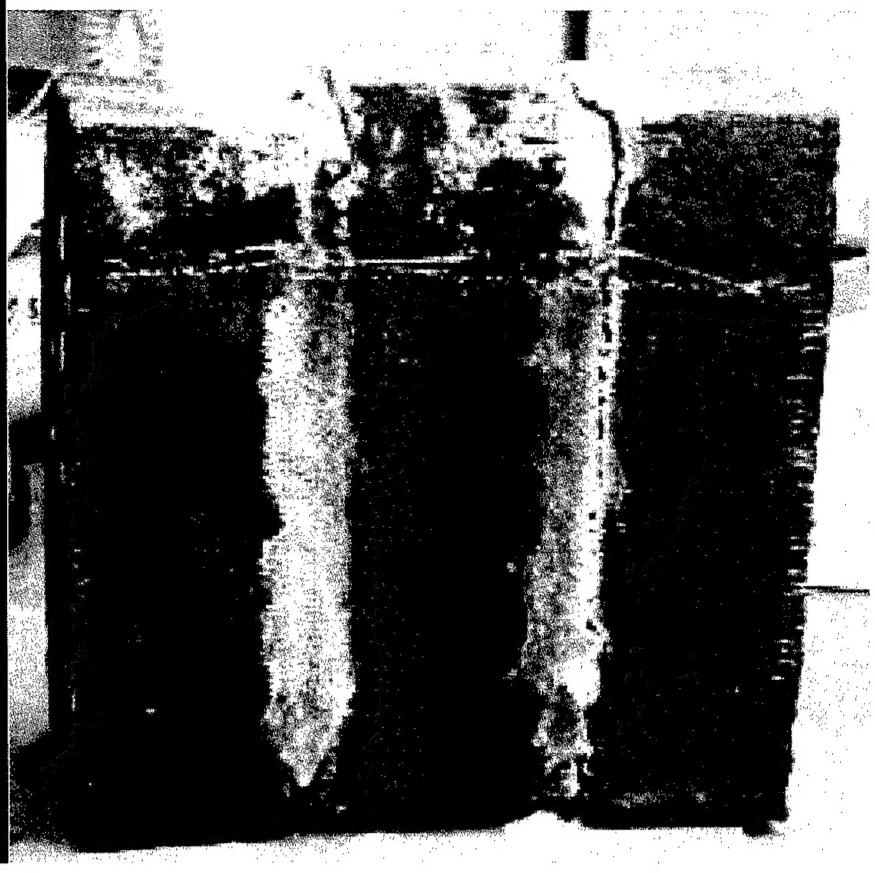

20030303 056

Approved for public release; distribution is unlimited.

ERDC TR-02-7

Construction Engineering Research Laboratory

US Army Corps of Engineers®
Engineer Research and Development Center

Biaxial Loading and Failure Behavior of Brick Triplets with Fiber-Reinforced Polymer Composite Upgrades

J.B. Berman, G.K. Al-Chaar, and P.K. Dutta

December 2002

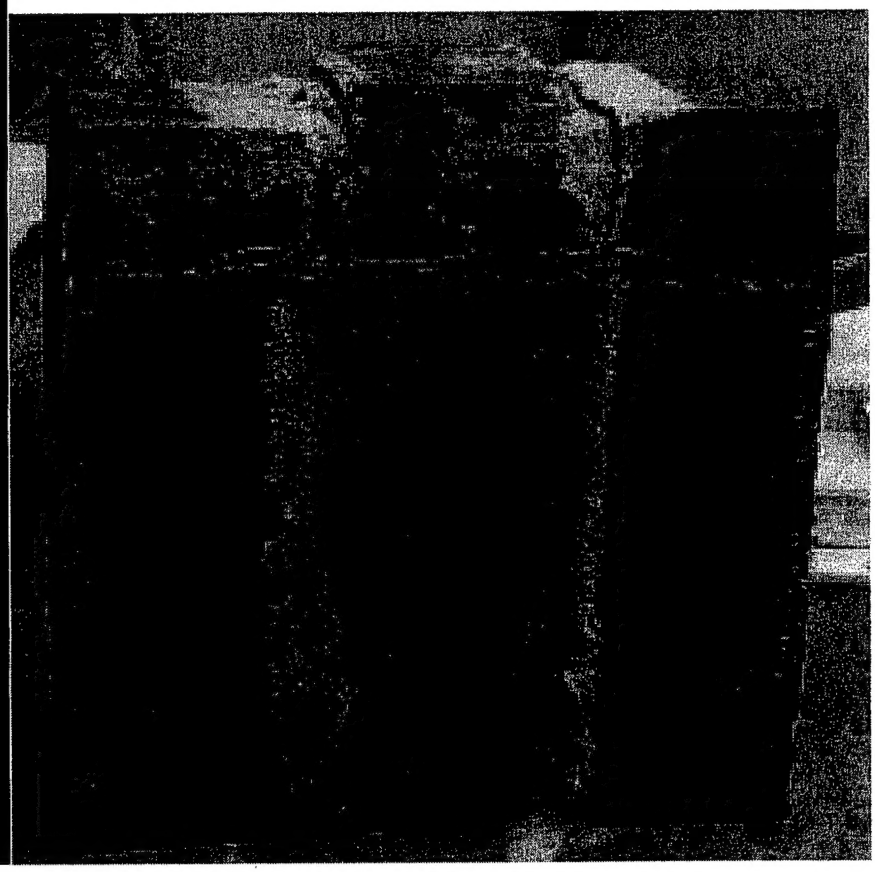

Approved for public release; distribution is unlimited.

Foreword

This research was conducted for Headquarters, U.S. Army Corps of Engineers under Project 40162784AT41, "Military Facilities Engineering Technology"; Work Unit CFM-A081, "Accelerated Testing and Weathering of Structural Repair and Upgrade Composites." The technical monitor was David C. Bohl, CECW-EW).

The work was performed by the Materials and Structures Branch (CF-M) of the Facilities Division (CF), Construction Engineering Research Laboratory (CERL). The CERL Principal Investigator was Dr. Justin B. Berman.. The technical editor was Gordon L. Cohen, Information Technology Laboratory. Martin J. Savoie is Chief, CEERD-CF-M, and L. Michael Golish is Chief, CEERD-CF. The Technical Director of the Facility Acquisition and Revitalization business area is Dr. Paul A. Howdyshell, CEERD-CV-ZT, and the Director of CERL is Dr. Alan W. Moore.

A portion of this work and matching resources were provided by Dr. Piyush K. Dutta, Cold Regions Research and Engineering Laboratory (CRREL), Hanover, NH. CRREL work included triplet sample preparation and manufacturing by Rosanne L. Stoops; biaxial test fixture design by Dennis J. Lambert; and testing, data capture and sensor placement by Glenn D. Durell. In addition, CERL research assistants Mr. Jason M. Kamphaus, Mr. Aaron W. Nathan, and Mr. Stephen G. Hammill assisted with data analysis and report generation.

CERL and CRREL are elements of the Engineer Research and Development Center (ERDC), U.S. Army Corps of Engineers. The Commander and Executive Director of ERDC is COL John W. Morris III, EN, and the Director is Dr. James R. Houston.

DISCLAIMER: The contents of this report are not to be used for advertising, publication, or promotional purposes. Citation of trade names does not constitute an official endorsement or approval of the use of such commercial products. All product names and trademarks cited are the property of their respective owners. The findings of this report are not to be construed as an official Department of the Army position unless so designated by other authorized documents.

DESTROY THIS REPORT WHEN IT IS NO LONGER NEEDED. DO NOT RETURN IT TO THE ORIGINATOR.

Contents

List of Tables and Figures

Tables

Figures

1 Introduction

1.1 Background

In order to protect personnel and assets from the effects of earthquakes, the U.S. Army has sponsored investigation of various structural rehabilitation technologies suitable for retrofit application to unreinforced masonry buildings. One promising emerging technology is the application of fiber-reinforced polymer (FRP) composites to various unreinforced brick and concrete block configurations. Structural rehabilitation using FRP composites has repeatedly been shown to be an effective way to improve masonry panel strength and ductility at a relatively low cost [Al-Chaar and Hasan 1998; Marshall 2000].

During an earthquake or other ground motion, masonry panels must resist both lateral and gravity loads. Reliable prediction of masonry panel shear capacity is important both in estimating wall performance and in developing cost-effective retrofit designs. Prediction of capacity is highly sensitive to the mode of failure, and this is strongly influenced by the normal (i.e., gravity) load on the panels.

Structural performance tends to be calculated either through small-scale testing of system constituents, such as concrete cylinders and FRP sample coupons, or system-level testing of a large scale model. Small-scale tests are affordable, but the results tend to be simplistic in terms of real-world structural performance; large-scale tests can account for many complex variables to produce reliable, verifiable results, but the cost in terms of time and resources is often prohibitive. The structural engineering community could benefit from a testing protocol that combines the best aspects of both large- and small-scale testing while minimizing the disadvantages of each. One candidate for such a test is the *triplet test*.

The triplet test is a sub-system test that can offer a better understanding of a masonry wall's shear strength than can a coupon test, especially when the mode of failure is cracking through the mortar joints. A triplet test differs from ASTM International's Diagonal Tension Test [ASTM E519-81], which is used to determine the shear strength along a failure line through both mortar and masonry unit and which simply represents an average value for the specimen. In contrast, the triplet test also identifies the lower boundary of the specimen's shear strength because it

measures shear resistance along the mortar joint, which is typically lower than the value for brick.

To be useful, a triplet test should be designed to reflect loads and stresses that will affect the sub-system in a real-world structure. The test methodology should be consistent and standardized, and should minimize or eliminate variances among triplets in terms of basic physical configuration, the way loads are applied, etc. In order to accomplish realism and uniformity, triplet tests should prescribe loads that are comparable to the expected real-world normal load, with consideration for the fact that 'normal' load varies from the bottom of a wall to the top. Applying a surrogate normal load perpendicular to shear not only helps to simulate actual conditions in the field, but also prevents unrealistic (i.e., irrelevant) shear failure modes that would occur in uniaxial in-plane shear testing of the triplet. In triplet testing, the application of a surrogate normal load forces the failure to occur as true shear rather than a complex combination of forces resulting from imperfections or inconsistencies in controlling test conditions.

In addition to supporting an AT41 project entitled "Seismic Rehabilitation of URM Walls," which concluded in Fiscal Year 2002, this investigation was intended to enhance engineering knowledge about predicting the shear capacity of masonry structures under various levels of normal loading. The study produced data that will be valuable in any future efforts by government or industry to standardize the triplet test as a means to describe the mechanical properties of masonry panels.

1.2 Objective

The objective of this work was to study the behavior of masonry triplet samples, both unreinforced and reinforced to different degrees with FRP composites, under biaxial in-plane loading.

1.3 Approach

One-hundred triplet samples were constructed using three standard brick units each, nominal dimensions 8 x 2½ x 4 in. The bricks were connected using 3.8 in. joints of N-type mortar made of portland cement, lime, and sand in proportions of 1:1:6 by volume, respectively. The middle brick in each triple was offset 0.5 in. relative to the adjacent bricks to provide load transfer from the exterior brick surfaces to the mortar joints during lateral (shear) loading.

Some triplet samples were reinforced with FRP overlays, which consisted of glass / epoxy patches measuring 2 x 7.5 in. These patches were applied across all three brick courses to within 1/8 in. of the surfaces designated to bear the compressive (normal) load. This specification ensured that the entire surrogate normal load was carried by brick only, with no help from the FRP material.

The samples were organized into three test series, designated Series 0, I, II. Series 0 had no FRP patches applied; Series I triplets had an FRP patch applied on one side only; Series II triplets had an FRP patch applied to both sides.

Each series was organized into six sets of five samples that were identified in terms of the applied normal load as a percentage of the normal load capacity. For example, the I-100 set comprised triplets with FRP applied on one side and tested to failure under normal load only; the 0-12.5 set had no FRP reinforcement and was tested with an applied normal load of 12.5% normal capacity during lateral loading to failure. In addition, six specimens were tested using a linear variable displacement transducer (LVDT) using 3.0% normal loading, comparable to a one-story brick building under a pure gravity load. Load-displacement curves were generated, compared, and compiled into performance envelopes.

1.4 Mode of Technology Transfer

The following modes of technology transfer are recommended or already in progress:

1. Condensed triplet data and failure envelopes generated from this study have been transferred to the ERDC/CERL structural engineering team for incorporation into or revision of documentation of the AT41 project entitled "Seismic Rehabilitation of URM Walls." Such documentation may include guide specifications or other criteria documents.
2. The results of this study will be published as a peer-reviewed conference paper and journal publication to provide a broader context for the knowledge gained from this research and to highlight possible Army and non-Army applications.
3. A recommendation will be made to ASTM to evaluate the viability of the biaxial triplet test as an effective and valid method for qualifying the in-plane performance of masonry walls, both unreinforced and reinforced.

1.5 Units of Weight and Measure

U.S. standard units of measure are used throughout this report. A table of conversion factors for Standard International (SI) units is provided below.

SI conversion factors		
1 in.	=	2.54 cm
1 oz	=	29.574 ml
1 gal	=	3.78 L
1 lb	=	0.453 kg
1 kip	=	453 kg
1 psi	=	6.89 kPa
°F	=	(°C x 1.8) + 32

2 Experimental Design, Results, and Discussion

2.1 Overview

This chapter documents background research (i.e., a survey of relevant literature), specimen preparation, test setups, and results of all 100 triplet sample tests. Figures 1 – 4* illustrate the design of the brick triplet specimens and the experimental setup. The loads at yield and ultimate failure, and their corresponding displacements, are summarized in Tables 1 – 4. The observed modes of failure for each sample are summarized in Tables 5 – 7 and Figures 5 – 8. The effect of different normal loads and the two different FRP application schemes are explained in detail. The results are analyzed in terms of capacity and displacement.

2.2 Literature Survey

As indicated in Chapter 1, it is more expedient and practical to test subsystem components than to test at the system-level using full-scale equivalents. A subsystem test allows for better control of the testing parameters and, due to its scale, makes multiple tests affordable. To date, the triplet test is one of the simplest tests for assessing the shear strength of masonry walls. The triplet test consists of three clay bricks each separated by a mortar joint. For shear testing, the center brick is often offset by ½ in., but this offset is not necessary for assessing impact or normal stress behavior.

The first mention of triplet testing in the literature dates back to 1988, when a paper discusses the triplet test as a possible predictor of brick/mortar interface shear strength [Ghazali and Riddington 1998]. The same paper discusses the possible use of a Mohr-Coulomb model to perform additional biaxial predictions (shear

* All tables and figures are presented after the main text of this report.

stress/normal stress space). Since that time, various studies have explored the effect of impact stress rate [Molyneaux 1994; Beattie 2001], support conditions [Beattie et al. 2001; Bouzegoub et al. 1995], and substrate type [Marzahn 1997] on triplet shear strength. Additional works have explored the effect of bed joint type and thickness on the triplet normal strength [Hughes and Kitching 2000]. In 1996 the research community began to explore the triplet test's utility in determining the effectiveness of FRP upgrades [Saadatmanesh et al. 1997; Saadatmanesh and Ehsani 1996]. Presently, a variety of works look at the effect of FRP laminate thickness and width [Marshall et al. 2000], FRP rod placement [Tinazzi et al. 2000], and concrete laminate placement [Marshall 2002] on shear strength. In summary, the literature encompasses a wide range of research using triplets as the base test, but no work has addressed the biaxial testing of FRP-reinforced triplets.

2.3 Sample Preparation

All triplets were constructed and prepared under controlled laboratory conditions. Standard red clay bricks were used along with a type N mortar and constructed as shown in Figure 1. The mortar was allowed to cure 30 days before application of FRP and/or testing of the triplets. Prior to FRP application all samples were thoroughly cleaned with a wire brush using at least 60 strokes on both sides of the triplet.

The FRP consisted of a plain weave E-glass fabric embedded in an epoxy resin. The epoxy used was a standard room-temperature-cure bisphenol A epoxide with a polyamine curing agent. The epoxide was mixed in approximately 22.9 oz batches at a mix ratio of 3.75:1 by weight.

A thin layer of epoxy was used to prime either one side or both sides of Series I or Series II triplets, respectively. The wetted fabric was then placed and followed by a second layer of epoxy. Using this procedure, each FRP-reinforced triplet received approximately 1 oz of resin per side coated. Intimate contact between FRP and triplet was established using a corrugated aluminum roller applied to the surface of the pre-cured FRP. Two days were allowed to pass before testing the FRP-upgraded triplets to allow a complete cure.

All samples were tested biaxially such that the normal load was controlled to reflect percentage of its normal load capacity while the shear load is applied to failure (Figure 2). The test setup is shown in Figure 3.

In order to estimate basic material properties of the tested specimens, six samples were instrumented with LVDTs as shown in the Figure 4. Two samples of Series 0, I, and II were instrumented. One LVDT for measuring shear strain over a 5.0 in. length of the mortar joint as the normal load was applied at 3.0% normal load capacity for the given series. One LVDT was also placed across the two joints to measure the compressive strain across the joint between the centerlines of the two exterior bricks as the normal load is applied at 3.0% normal load capacity for the given series.

2.4 Triplet Load Response

2.4.1 Capacity at Normal Load

Table 8 illustrates the effect of normal load on the capacity of specimens without FRP (Series 0), with FRP (Series I) applied to one side, and FRP applied to both sides (Series II). It is clear from this table that the application of normal load to the specimen increased the shear capacity significantly for all specimen types. For Series I specimen loaded at 25% normal capacity, the shear capacity increased by a factor of 6.32. For a Series I and II specimens loaded at 25% normal capacity, the shear capacity increased by factors of 2.60 and 2.66, respectively.

Another observation from Table 8 is that under normal loading, the relative gain in shear capacity was lower for the FRP-upgraded specimens than for the Series 0 triplets. This is evident from the example cited in the previous paragraph, and the same trend holds true for every normal loading applied during the tests.

Table 8 also illustrates the large difference between shear (lateral) load capacity and normal (crushing) load capacity. For a specimen without FRP, the shear capacity was 3.1 kips while the normal load capacity was 36.7 kips – a twelve-fold difference. However, the actual amount of normal loading applied did not have an appreciable effect on shear capacity as long as at least the minimal normal load was applied. For example, a Series 0 specimen under normal loads of 25%, 50%, and 75% exhibited respective shear capacity increases of 6.32 times, 6.09 times, and 6.18 times the value for pure shear. This trend is strongly supported by results for the other two specimen types.

2.4.2 Displacement at Normal Load

Table 9 illustrates the effect of normal load on lateral displacement at peak load for different FRP applications. The first observation from this table is that applying

normal load of any value increases the ultimate displacement of the triplet specimens. However, the amount of increase in ultimate displacement decreases as the normal load increases. For example, a Series 0 specimen has an ultimate displacement of 0.034 in. in pure shear. With 25% normal load, the ultimate displacement increases by a factor of 13.13, but the relative amount of increase in ultimate displacement then decreases as the normal load increases up to 100% normal capacity, at which point the increase factor drops to 3.52. These trends are evident for all specimen types and normal loads.

The other observation from Table 9 is that the relative increase in ultimate displacement for different normal loads decreases as the amount of FRP increases. For instance, a Series 0 specimen under 25% normal load increased in ultimate displacement by a factor of 13.13 with respect to the pure shear loading case. Under that same normal load, the ultimate displacement of a Series I specimen increased by a factor of only 6.77. The ultimate displacement for a Series II triplet only increased by a factor of 4.47 under the same normal loading.

2.4.3 Load-Displacement Response

Load-displacement curves are shown in Figures 9 – 14. The raw data for the five samples graphed for each load level are plotted along with a linear (or bilinear) fit. The fitted curves were developed by plotting the origin of the axis against the value where the average peak loads and displacements occurred (determined from Table 1). In some cases, as in Figure 9, initial data have been removed to adjust for the initial upward concavity of the curve due to initial load settling. With this information it is observed that in Figures 9 and 10, brittle failure is indicated by both curves under 100% normal load and under 0% shear load. Bilinear curves are observed in Figure 11 and 12 under 12.5% and 25% normal load levels, respectively. At higher normal load levels the failure transfers from bilinear (25% normal load) to slightly bilinear (50% normal load, shown in Figure 13) to completely linear again (75% normal load, shown in Figure 14).

2.5 Effects of FRP on Triplet Behavior

The FRP application scheme had significant impacts on triplet behavior. The following discussion summarizes the behavior in terms of strength and ductility. For purposes of this discussion, displacement reached at peak load is used as a surrogate measure of ductility.

2.5.1 Capacity

Table 10 shows the capacity of Series 0, I, and II specimens under different normal loads.

Under pure shear (i.e. no normal loading), FRP increased the shear capacity by 46% and 120% for Series I and Series II applications, respectively. However, when a normal load was applied, the shear capacity of FRP-upgraded triplets actually tended to decrease. For Series I triplets, shear capacities at ultimate decreased by an average of 15.4% for normal loads of 12.5%, 25%, 50%, and 75% as compared to the bare specimen values. For Series II triplets under normal loads, the shear capacity essentially remained constant, exhibiting a slight average drop of 0.7%.

Under pure normal load at 100% capacity, the crushing strength for a bare Series 0 specimen averaged 36.7 kips. An average decrease in normal capacity of 9% was observed for Series I specimens, while normal capacity remained approximately constant (2% average increase) for Series II specimens. Based on the data scatter observed in these results, all values are essentially equivalent from a statistical standpoint. This indicates that FRP contributed little to normal load capacity.

Therefore, in every test that included any normal load component, the application of FRP decreased shear capacity as compared with bare specimens. In the Series II specimens, however, the decrease in capacity was negligible.

2.5.2 Displacement at Peak Load

Table 11 illustrates the displacement at peak load for Series 0, I, and II specimens under different normal loads. Contrary to the discussion concerning the effects of FRP on capacity, no clear trends were identified with respect to the effects of FRP on displacement at peak load. For pure shear, the addition of FRP doubled the value of ultimate displacement. When normal load was applied, the ultimate displacement ratio decreased for normal loads of 25% and 75%, but increased for 50% normal load. Clearly, the main factor affecting ultimate displacement is the amount of normal load rather than whether or not FRP was applied.

2.5.3 Load-Displacement Response

Load-displacement curves are shown in Figures 15 – 20, for Series I, and in Figures 21 – 26 for Series II. In Figures 15, 16, 21, and 22, brittle failure is observed in both curves under 100% normal load and under 0% shear load. As seen in the Series 0 triplets, bilinear curves are observed under 12.5% and 25% normal load levels for

both series. Also, at the higher normal loads of 50% and 75%, the same transitioning from bilinear failure behavior to brittle (linear) material behavior is observed. As with Series 0, Series I and II use a similar linear and bilinear curve-fitting scheme.

As shown in Table 10, when normal loads of 12.5% or higher is applied, Series I exhibits higher shear loads at ultimate than Series 0. It is also observed in Table 11 that Series I exhibits higher displacements than Series 0 and Series II.

The curves for all Series II samples under pure normal loading are less staggered than those for Series 0 and I. The presence of FRP on both sides of the samples led to consistent failures.

2.6 Triplet Properties

Figures 27 – 32 show the variation in normal and shear strain versus time. The measured strains at half of ultimate are summarized in Table 12. The strains (normal and shear) were sampled at the five points immediately around $t = 200$ seconds during the test. The average strains were calculated from those data and the ratio provided an effective Poisson's ratio. One important item to note is that while the vertical strain is listed as positive during the test, it is actually of negative sign and hence, the Poisson's ratio, $-\varepsilon_n/\varepsilon_v$, requires a sign change. From the data, it is concluded that the FRP alters the effective Poisson's ratio for triplet. The results for the the Series 0 and Series I triplets are reasonable. However, the Series II triplets show a dramatically reduced Poisson's ratio. This Series II result shows an overall lower normal strain compared to the other two series. This is probably due to the fact that the FRP applied to both sides of the triplet provides full normal constraint of the mortar joint, which therefore requires much greater stress to open the joint. This manifests itself as a reduced normal strain, hence reduced effective Poisson's ratio. Further validation for these observations should be explored through additional testing.

Figures 33 – 38 show the stress-strain curves for samples with LVDTs. The Series 0 samples had an average strain to yield of 64.5 $\mu\varepsilon$. This is an order of magnitude lower than Series I and II, which had average strains to yield of 782 $\mu\varepsilon$ and 123 $\mu\varepsilon$, respectively. This difference is to be expected as the woven E-glass/epoxy composite increases the overall ductility of the reinforced triplets. Using the stress-strain data for the elastic portion up to yield, the effective shear modulus can be calculated. While, the data sampling rate does not provide a good resolution of data to predict this behavior, the stress levels used along with the above strains indicate that the

effective shear modulus for the Series 0 triplet is at least an order of magnitude greater than triplets with FRP reinforcement.

Figures 39 through 44 are bilinear curve fits for the averaged load-displacement data points of all series at 0% through 100% normal load. The results are plotted as average load-displacement curves. No effort has been made to convert the data to stress-strain since strain gages were not used and accurate areas for load distribution are unknown. However, the base load-displacement curves can all be represented by the following generic bilinear relationship:

$$P_v = \begin{Bmatrix} a_0\delta & \delta \le \delta_{cr} \\ b_0\delta + b_1 & \delta_{cr} \le \delta \le \delta_{ult} \end{Bmatrix} \quad (1)$$

where δ_{cr} is the bilinear point of inflection and is defined as

$$\delta_{cr} = \frac{b_1}{a_0 - b_0} \quad (2)$$

and a_0, b_0, b_1 and δ_{ult} are the four bilinear curve-fitting parameters. The parameters for Figure 39 – 44 are summarized in Table 13. Figure 45 – 47 present the average load-displacement curves, ranging from 0% through 100% normal load for each given series. Again, the fitting parameters for these equations can be found in Table 13.

2.7 Triplet Failure Modes

The failure modes of the various triplet series were captured in Figures 5 – 8 and discussed in detail in Tables 4 – 7. The resulting normal load versus shear load failure envelopes, along with their associated standard deviations, are provided for Series 0, I, and II in Figures 48, 49, and 50, respectively. One item to observe is that near the lower normal load levels, sometimes two points are plotted for a given normal load. This represents deviations in bilinear yield and ultimate failure loads. The reasoning for this difference is discussed below.

One commonality found in all three triplet series is that the presence of a normal load below 12.5% produces a general increase in shear capacity followed by shear failure of the brick/mortar interface. This increase in shear load is due to internal friction and is coincident with the Mohr-Coulomb phenomenon. This can be frictional force between the masonry and the mortar (in Series 0) or between the masonry, mortar, and FRP (in Series I and II). This phenomenon has been docu-

mented in load-displacement Figures 11, 17, and 23, as is noted by the second low-slope portion of the bilinear response. To a lesser extent, Figures 12, 18, and 24 illustrate similar behavior for the series under 25% normal loading, but the greater slope indicates that there are other mechanisms at play.

Between 12.5% and 25% normal loads, an interesting mixed-mode behavior occurs. As evident by the load-displacement curves found in Figures 12, 18, and 24, the specimens still exhibit the bilinear behavior. The bilinear behavior in this case is partially due to internal friction and partially due to the onset of transverse brick cracking. At the first failure point, the mortar has separated from the brick (and sometimes the FRP). Frictional forces dominate, but the large normal load redirects the principle stresses into continued transverse brick cracking. The combined friction slip and transverse brick cracking leads to the slightly positive slope in the second bilinear portion of the curve. In most of the 12.5% and 25% normal load figures, the bilinear response continues until the center brick has displaced the full offset distance of 0.5 in.

Above 25% normal load, the failure mode has almost transitioned completely to transverse brick cracking. The high normal stresses set up cracks that propagate through the brick with the onset of any shear displacement. The result is a decreasingly bilinear behavior transitioning to a low-displacement, relatively linear (e.g. brittle) response. From 75% normal load and beyond, nearly all signs of bilinearity are gone as compressive brick crushing dominates.

A summary of the normal load versus shear load failure envelopes for all Series 0, I, and II triplets is superimposed and provided in Figure 51. It is observed in Figure 51 that the FRP resulted in higher shear value at a low normal load of (12.5%) and lower shear value at higher normal loads (greater than 25%). One explanation for this phenomenon is that the presence of FRP results redirects the loads at high normal stress levels to the weakest load path, hence resulting in earlier failure. Figure 52 shows the data presented in Figure 51 presented as normalized failure envelopes. The figure illustrates how the failure envelopes separate further when normalized versus absolute values are presented.

2.8 Triplet Failure Criteria

With the mechanical testing of triplets that consist of mortar and brick, several brittle failure mechanisms are possible, so several failure criteria must be considered. Under increasing normal load, one expects friction to increasingly dominate in the failure of the system. As indicated previously, data show that internal friction

dominates for normal loads at least up to 12.5% normal capacity but not greater than 25% normal. Hence, up to 12.5% normal strength loading, the simple Mohr-Coulomb expression below can be applied to predict triplet yield failure:

$$\sigma_v = \mu\sigma_n + \sigma_v^0 \tag{3}$$

$$\text{for } 0 \le \sigma_n \le 0.125\sigma_n^0$$

where

$$\sigma_v = \frac{P_v}{2A_{\text{int}}};\ \sigma_v^0 = \frac{P_v^0}{2A_{\text{int}}};\ \sigma_n = \frac{P_n}{A_{\text{int}}} \tag{4}$$

where A_{int} is the brick/mortar overlap area and σ_n^0 is the normal strength intercept (value at zero shear loading). Also, the shear failure strength, σ_v, can be related directly to the normal strength using two independent variables: μ, the friction coefficient, and σ_v^0, the shear strength intercept (value at zero normal loading). These two variables are only functions of the substrate materials (brick, mortar) and the bonded reinforcement (FRP). Hence, one can take the data points for yield captured in the experiment up to 12.5% normal failure strength and apply the expression above to define the variables as shown in Table 14.

Very little literature has been published on brick/mortar friction coefficients. Available sources quote values as low as 0.3 [Alcocer and Zepeda 1999] and as high as 1.20 [Marzahn 1998; Marzahn 1996]. In this study, the measured value for the triplet without FRP (0.795) fits comfortably between these two extremes. In addition, the introduction of an FRP material to oneside increases the apparent frictional coefficient, which is an anticipated result. However, the decreased coefficient for the introduction of FRP to both sides of the sample may be an additional indicator that failure initiates and occurs along a different load path than the brick/mortar joint.

While μ has not been well documented, papers have experimentally characterized σ_v^0 for various rehabilitated triplets [Marshall 2002; Marshall et al. 2000; Marshall et al. 1999; Saadatmanesh et al. 1997]. The σ_v^0 values in Table 14 provide numbers consistent with Marshall et al. [1999], which predicts 42.8 psi for triplets without FRP (22% difference) and 91.1 psi for triples with 2 in. glass FRP applied to one side (14% difference).

To develop the ultimate failure criterion for the full quadrant behavior in the triplet, a broader generalized model is needed. The simple linear relationship, as presented in the Mohr-Coulomb model (equations 3 and 4), is insufficient to describe

the full envelope of behavior for two reasons. First, it only adequately describes the failure mode up to yield and not from yield to ultimate, which is indicative of the bilinear behavior. Second, transverse cracking within the brick from 25% normal load and beyond renders the equation invalid. However, for the generalized failure model, the data for each of the three series can be expressed as a quartic equation and still correlate with data at greater than $r = 0.99$:

$$\sigma_v = a_5\sigma_n^4 + a_4\sigma_n^3 + a_3\sigma_n^2 + a_2\sigma_n + a_1 \tag{5}$$

$$\text{for } 0 \le \sigma_n \le \sigma_n^0$$

where a_1, a_2, a_3, a_4, and a_5 are the five curve-fitting parameters. The results are given in Table 14.

Figure 53 presents the normal load versus shear load failure envelopes along with the Mohr-Coulomb and Generalized Failure Criteria models.

3 Conclusions

One hundred brick triplets were tested under combined shear and normal loading in order to evaluate standard and FRP-reinforced configurations. The results indicate that the triplet test can provide an estimate of the shear capacity and failure modes of masonry wall systems in the field. From the results documented in this report, ten overall observations are made:

1. The application of normal load significantly increased the shear capacity of each specimen series.
2. The relative gain in shear capacity decreased with the addition of FRP for any given normal load.
3. Under pure shear, the application of FRP to the specimen increased the shear capacity. However, when normal loads were applied, the shear capacity decreased when FRP was introduced, especially for Series I specimens.
4. As the normal load increased from 25% to 75%, the shear capacity remained approximately constant for each specimen type.
5. Applying normal load increased the ultimate displacement of all specimens with respect to the pure shear loading case.
6. The relative gain in ultimate displacement, with respect to the pure shear case for each specimen type, decreased as the amount of normal load increased from 25% to 100%.
7. For any given normal load, the relative gain in ultimate displacement, with respect to the pure shear case, decreased as the amount of FRP increased.
8. The application of FRP increased the ultimate displacement for the pure shear loading case. However, when normal loads were introduced, no clear trend in ultimate displacement was evident.
9. Since most brick walls will be subjected to only 4 – 6% relative to ultimate load due to gravity loading, the Mohr-Coulomb model is sufficient for predicting masonry wall triplet yield failure loads.
10. A generalized quartic model is sufficient for predicting masonry wall triplet ultimate failure loads for 0% to 100% normal loading.

References

Al-Chaar, Ghassan K., and Husein Hasan. June 1998. *Masonry Bearing and Shear Walls Retrofitted With Overlay Composite Material: Seismic Evaluation and Dynamic Testing*, ERDC/CERL Technical Report (TR) 98/86.

Alcocer, S.M., and J.A. Zepeda. 1999. "Behavior of Multi-Perforated Clay Brick Walls under Earthquake-type Loading," *Proceedings of the 8th North American Masonry Conference*, 6-9 June 1999, Austin, TX, pp 235 – 246.

ASTM E 519-00. *Standard Test Method for Diagonal Tension (Shear) in Masonry Assemblages*, pp 1138 – 1142.

Beattie, G., T.C.K Molyneaux, M. Gilbert, and S. Burnett. 2001. "Masonry Shear Strength under Impact Loading," *Proceedings of the 9th Canadian Masonry Symposium*, 4-6 June 2001, Fredericton, New Brunswick, Canada, pp 2C29:1 – 12.

Bouzegoub, M.C., P. Jukes, and J.R. Riddington. 1995. "Influence of Loading Arrangement on the Initial Mode of Failure of Brick Specimens," *Computer Methods in Structural Masonry – 3*, Eds. J. Middleton and G.N. Pande, Books and Journals International, pp 117 – 126.

Ghazali, M.Z., and J.R. Riddington. 1988. "Simple Test Method for Masonry Shear Strength," *Proceedings of the Institution of Civil Engineers, Part 2 - Research and Theory*, No. 85, September 1988, pp 567 – 574.

Hughes, T.G., and N. Kitching. 2000. "Small Scale Testing of Masonry," *Proceedings of the 12th International Brick/Block Masonry Conference*, 25-28 June 2000, Madrid, Spain, pp 893 – 902.

Marshall, O.S. March 2002. *Test Report on CMU Wall Strengthening Technology*, ERDC/CERL Letter Report LR-02-1.

Marshall, O.S., S.C. Sweeney, and J.C. Trovillion. June 2000. *Performance Testing of Fiber-Reinforced Polymer Composite Overlays for Seismic Rehabilitation of Unreinforced Masonry Walls*, ERDC/CERL Technical Report, TR-00-18/ADA381207.

Marshall, O.S. Jr., S.C. Sweeney, and J.C. Trovillion. 1999. "Seismic Rehabilitation of Unreinforced Masonry Walls," *Fourth International Symposium Fiber Reinforced Polymer Reinforcement for Reinforced Concrete Structures* (ACI SP-188), ACI International, Farmington Hills, MI, pp 287 – 295.

Marzahn, G. 1998. "The Shear Strength of Dry-Stacked Masonry Walls," Leipzig Annual Civil Engineering Report, Leipzig, Germany, no. 3, pp 247 – 261.

Marzahn, G. 1997. "Shear Strength of Grout-Dowelled Masonry," Leipzig Annual Civil Engineering Report, Leipzig, Germany, no. 2, pp 335 – 352.

Marzahn, G. 1996. "Improving the Shear Bond Behaviour of Masonry," Leipzig Annual Civil Engineering Report, Leipzig, Germany, no. 1, pp 245 – 268.

Molyneaux, T.C.K. 1994. "Vehicle Impact on Unreinforced Masonry Parapets," *Proceedings of the Public Highways Agency Maintenance Engineers Conference*, 5 – 7 September 1994, Southwark St., London.

Saadatmanesh, H., M.R. Ehsani and A. Al-Saidy. 1997. "Shear Behavior of URM Retrofitted with FRP Overlays," *Journal of Composites for Construction*, vol 1, no. 1, pp 17 – 25.

Saadatmanesh, H., and M.R. Ehsani. 1996. "Repair and Strengthening of Earthquake-Damaged Concrete and Masonry Walls with Composite Fabrics," *Proceedings of the First International Conference on Composites in Infrastructure (ICCI '96)*, 15 – 17 January 1996, Tucson, AZ, pp 1156 – 1167.

Tinazzi, D., C. Modena, and A. Nanni. 2000. "Strengthening of Masonry Assemblages with FRP Rods and Laminates," International Meeting on Composite Materials, PLAST 2000, *Proceedings of Advancing with Composites 2000*, 9 – 11 May 2000, Crivelli-Visconti, Italy, pp 411 – 418.

Tables and Figures

Table 1. Load-displacement summary of Series 0 test samples.

Group ID	Sample No.	Load at Yield (lb)	Displacement at Yield (in.)	Ultimate Load (lb)	Displacement at Ultimate (in.)
0-0	1	3235	-	3235	-
0-0	2	3260	-	3260	-
0-0	3	2895	0.039	2895	0.039
0-0	4	2593	0.029	2593	0.029
0-0	5	3971	0.032	3971	0.032
0-0	6	2823	0.029	2823	0.029
0-0	7	2629	0.043	2629	0.043
0-12.5	1	6955	0.089	8170	0.497
0-12.5	2	9753	0.106	10809	0.497
0-12.5	3	12753	0.168	11188	0.444
0-12.5	4	11301	0.153	14520	0.376
0-12.5	5	12711	0.113	13858	0.424
0-25	1	15218	0.236	18907	0.446
0-25	2	11382	0.150	19715	0.469
0-25	3	13224	0.154	20226	0.491
0-25	4	10672	0.117	18501	0.430
0-25	5	12903	0.194	19268	0.416
0-50	1	17572	0.113	17572	0.113
0-50	2	19844	0.154	19844	0.154
0-50	3	20064	0.125	20064	0.125
0-50	4	19153	0.279	19153	0.279
0-50	5	16462	0.140	16462	0.140
0-75	1	15658	0.169	15658	0.169
0-75	2	21172	0.123	21172	0.123
0-75	3	18937	0.169	18937	0.169
0-75	4	20310	0.162	20310	0.162
0-75	5	18341	0.115	18341	0.115
0-100	1	35760	-	35760	-
0-100	2	36980	-	36890	-
0-100	3	41879	0.121	41879	0.121
0-100	4	35468	0.129	35468	0.129
0-100	5	44894	0.108	44894	0.108
0-100	6	25952	0.108	25952	0.108
0-100	7	35693	0.138	35693	0.138
0-LVDT	1	6729	0.071	9073	0.093
0-LVDT	2	9647	0.077	9717	0.080

Table 2. Load-displacement summary of Series I test samples.

Group ID	Sample No.	Load at Yield (lb)	Displacement at Yield (in.)	Ultimate Load (lb)	Displacement at Ultimate (in.)
I-0	1	4483	0.059	4483	0.059
I-0	2	4437	0.077	4437	0.077
I-0	3	5606	0.082	5606	0.082
I-0	4	3775	0.070	3775	0.070
I-0	5	3986	0.087	3986	0.087
I-12.5	1	15469	0.150	13907	0.497
I-12.5	2	7047	0.160	6805	0.468
I-12.5	3	10577	0.229	7196	0.574
I-12.5	4	12830	0.138	13730	0.451
I-12.5	5	17938	0.147	16220	0.543
I-25	1	15440	0.147	13906	0.497
I-25	2	6955	0.147	6805	0.468
I-25	3	10632	0.231	7196	0.574
I-25	4	12829	0.138	13729	0.451
I-25	5	17938	0.147	16220	0.543
I-50	1	18859	0.162	18048	0.198
I-50	2	15327	0.180	15327	0.180
I-50	3	14320	0.233	14108	0.242
I-50	4	20610	0.142	20267	0.222
I-50	5	16547	0.110	11258	0.220
I-75	1	12415	0.080	18286	0.160
I-75	2	13809	0.113	13742	0.132
I-75	3	16061	0.131	16061	0.131
I-75	4	19455	0.164	19455	0.164
I-75	5	13179	0.105	16144	0.149
I-100	1	39804	0.127	39804	0.127
I-100	2	26276	0.115	26276	0.115
I-100	3	28345	0.112	28345	0.112
I-100	4	36954	0.147	36954	0.147
I-100	5	35352	0.180	35352	0.180
I-LVDT	1	12726	0.115	12912	0.118
I-LVDT	2	8536	0.069	8862	0.088

Table 3. Load-displacement summary of Series II test samples.

Group ID	Sample #	Load at Yield (lb)	Displacement at Yield (in.)	Ultimate Load (lb)	Displacement at Ultimate (in.)
II-0	1	7393	0.085	7393	0.085
II-0	2	6704	0.067	6704	0.067
II-0	3	5732	0.082	5732	0.082
II-0	4	7224	0.078	7224	0.078
II-0	5	6604	0.082	6604	0.082
II-12.5	1	11774	0.172	13556	0.487
II-12.5	2	13480	0.173	19690	0.526
II-12.5	3	14270	0.155	11917	0.453
II-12.5	4	15485	0.105	7318	0.382
II-12.5	5	12396	0.107	10950	0.422
II-25	1	16217	0.155	17728	0.286
II-25	2	11215	0.118	19486	0.354
II-25	3	18906	0.325	18906	0.325
II-25	4	12405	0.173	14383	0.334
II-25	5	16373	0.132	19144	0.462
II-50	1	15623	0.185	15623	0.185
II-50	2	17373	0.218	17373	0.218
II-50	3	17514	0.230	16971	0.254
II-50	4	19401	0.210	19208	0.230
II-50	5	22251	0.139	22251	0.139
II-75	1	15188	0.170	15188	0.170
II-75	2	20853	0.167	20853	0.167
II-75	3	19109	0.120	19109	0.120
II-75	4	15639	0.124	15639	0.124
II-75	5	19838	0.119	19838	0.119
II-100	1	31577	0.109	31577	0.109
II-100	2	37033	0.105	37033	0.105
II-100	3	40634	0.112	40634	0.112
II-100	4	40210	0.128	40210	0.128

Table 4. Summary of Series 0 modes of failure.

Group	Sample	Modes of Failure 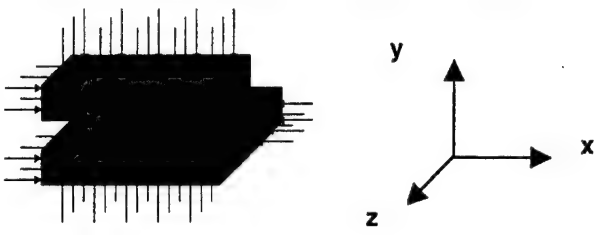
0-0	Al	A shear crack was visible along one mortar joint in the xz-plane
	3	Exhibited shear cracks in both mortar joints.
0-12.5	All	Shear cracks formed in both mortar joints. Tension cracks passed through the holes in the brick in the xy-plane. A single tension crack also appeared in the yz-plane of one exterior brick unit.
0-25	All	Shear cracks formed in each mortar joint in the xz-plane. Tension cracks appeared in the exterior brick units.
	4	Mode of failure was atypical. The specimen appeared to be loaded eccentrically causing a shear failure through the center brick and one exterior brick.
	5	Tension cracks materialized through the brick holes in the xy-plane.
0-50	1	Cracks initiated in the two mortar joints in the xz-plane. A small amount of corner spalling occurred at the loading end of the center brick.
	2	A tension crack was visible in the xy-plane of one exterior brick and the center brick. Tension cracks formed in the exterior bricks in yz-plane.
	3	Tension cracks appeared in the xy-plane of the two exterior brick and the center brick. Tension crack also formed in the interior brick unit in the yz-plane.
	4	Tension cracks were visible in the xy-plane of the two exterior bricks. Shear cracks materialized along one mortar joint in the xz-plane.
	5	Partial spalling occurred at the loading end of the center brick unit. A tension crack formed in the xy-plane of one exterior brick unit.
0-75	All	Partial spalling was observed at the loading end of the center brick. The confining pressure on the sample was high causing local failure at the loaded end. Several tension cracks also appeared in the yz-plane of one exterior brick unit.
0-100	All	Several tension cracks formed in the yz-plane along with spalling of the overhangs. (Note: Overhangs are not considered part of the prism area)

Table 5. Summary of Series I modes of failure.

Group	Sample	Modes of Failure
I-0	1, 3, 4, 5	Full debond between mortar joints and FRP was observed.
	2	Debond occurred between the mortar and the FRP along one mortar joint.
	3	A tension crack in the yz-plane was resisted by the FRP.
I-12.5	All	Specimens hardly intact after testing. All FRP was torn along the mortar joints.
	2	Severe tension cracks materialized in the center brick along the xy-plane.
	3	One exterior brick exhibited a shallow crack in xz-plane.
	4	Severe tension cracks formed in the center brick in the xy-plane. Tension cracks developed in both exterior bricks in the xy- and the yz-planes.
	5	One exterior brick contained two orthogonal cracks in the xy- and xz-planes.
I-25	All	Full debond between mortar joints and FRP was observed in all samples.
	1	One exterior brick contained a tension crack in the xy-plane and separation.
	2	The center brick and one exterior brick exhibited a tension crack in the xy-plane and separation.
	3	Spalling occurred at the edge of the loading end of the center brick.
	4	The area of debond between the FRP and the masonry was the largest for all samples. This indicated the center brick tended to move in the out-of-plane direction. One exterior brick exhibited cracks in the yz- and xy-planes through the top holes.
	5	The exterior bricks were cracked. One brick split in yz-plane while the other split as a result of diagonal (about 45 degrees) cracking.
I-50	All	Full debond between mortar joints and FRP occurred.
	1	A split in the center brick was observed in the xy-plane.
	2	A small amount of spalling was evident at one corner of the loading end of the center brick. Many cracks formed in the xy-plane of exterior bricks.
	3	Specimen was severely fractured as a result of tension cracks developing in the three bricks along the xy-plane.
	5	The edge of the center brick at the loaded end was chipped. Many tension cracks initiated in the exterior bricks along the yz-plane.
I-75	All	Full debond between mortar joints and FRP was observed in all samples.
	1	One corner of one exterior brick was chipped. A fracture formed in the center brick on the unprotected side. A tension crack materialized on the other exterior brick in the yz-plane.
	2	The extent of debond between the FRP and the mortar joints was the largest in the set. The center brick tended to move out-of-plane away from the FRP.
	3	Both exterior bricks developed one tension crack in the xy-plane.
	4	One exterior brick exhibited two tension cracks in the xy-plane.
	5	All bricks developed large tension cracks in the xy-plane.
I-100	1	Local debond was evident along one mortar joint due to premature failure in the loading end of the center brick accompanied by a tension crack in one exterior brick in the yz-plane.
	2, 4, 5	Full debond occurred between mortar joints and FRP.
	3	Debond initiated between the mortar and the FRP along one mortar joint. A longitudinal crack also formed in the adjacent exterior brick in the xy-plane.

Table 6. Summary of Series II modes of failure.

Group	Sample	Modes of Failure
II-0	All	Full debond between mortar joints and FRP occurred in all samples except Sample 5.
	5	The center brick totally debonded and one exterior brick contained a crack in the xy-plane.
II-12.5	1	Debond of the FRP on both sides along with spalling along the bottom of the center brick was observed.
	2, 3, 4	FRP was torn along both mortar joints.
	5	Debond between the FRP and one exterior brick occurred. Fracture of the loaded end of the central brick was observed. Orthogonal cracks developed along both xy- and yz-planes.
II-25	All	Full debond between mortar joints and FRP was observed. One or two cracks in the exterior brick formed along the yz-plane through the holes. Further cracking in the exterior bricks along the yz-direction was evident.
II-50	All	All exterior brick contained severe cracks in the xy-plane through the holes.
	1	Burst into several pieces upon failure.
II-75	All	The loading end of the center brick was chipped. Longitudinal cracks appeared in the exterior bricks along the xy-plane through the holes.
II-100	1, 2	Full debond between mortar joints and FRP was evident. Severe cracking and spalling occurred in the center brick. Tension cracks formed in the exterior bricks in xy- and xz-planes.
	3, 4, 5	Cracks developed in the xz-plane in all bricks outside the FRP surface.

Table 7. Summary of LVDT sample series modes of failure.

Group	Sample	Modes of Failure
0-LVDT	All	Shear cracks initiated in each mortar joint.
I-LVDT	All	A shear crack was evident in each mortar joint along with tears in the FRP.
II-LVDT	All	Shear cracks appeared in each mortar joint as well as tears in the FRP on both sides. A crack in one exterior brick formed in the xy-plane.

Table 8. Effect of normal load on shear capacity for different FRP applications.

	Shear Capacity for Different Normal Loads (kips)										
Series	0%	12.5%	Ratio*	25%	Ratio*	50%	Ratio*	75%	Ratio*	100%	Ratio*
Series 0	3.1	11.7	3.83	19.3	6.32	18.6	6.09	18.9	6.18	36.7	11.99
Series 1	4.5	11.6	2.60	11.6	2.60	15.8	3.55	16.7	3.76	33.3	7.48
Series 2	6.7	12.7	1.88	17.9	2.66	18.3	2.72	18.1	2.69	37.5	5.58

* Ratio of previous column to the capacity with 0% Normal Loading.

Table 9. Effect of normal load on displacement at peak load for different FRP applications.

	Displacement at Peak Load for Different Normal Loads (in.)										
Series	0%	12.5%	Ratio*	25%	Ratio*	50%	Ratio*	75%	Ratio*	100%	Ratio*
Series 0	0.034	0.448	13.04	0.451	13.13	0.162	4.73	0.147	4.29	0.121	3.52
Series 1	0.075	0.507	6.77	0.507	6.77	0.212	2.84	0.147	1.97	0.136	1.82
Series 2	0.079	0.454	5.76	0.352	4.47	0.205	2.60	0.140	1.78	0.112	1.42
* Ratio of previous column to the displacement at peak load with 0% normal loading.											

Table 10. Effect of FRP on shear capacity for different normal loads.

	Shear Capacity for Different FRP Applications (kips)				
Normal Load (%)	Series 0	Series 1	Ratio*	Series 2	Ratio*
0	3.1	4.5	1.46	6.7	2.20
12.5	11.7	11.6	0.99	12.7	1.08
25	19.3	11.6	0.60	17.9	0.93
50	18.6	15.8	0.85	18.3	0.98
75	18.9	16.7	0.89	18.1	0.96
100	36.7	33.3	0.91	37.5	1.02
* Ratio of previous column to the capacity with no FRP.					

Table 11. Effect of FRP on displacement at peak load for different normal loads.

	Displacement at Peak Load for Different Normal Loads (in.)				
Normal Load (%)	Series 0	Series 1	Ratio*	Series 2	Ratio*
0	0.034	0.075	2.18	0.079	2.30
12.5	0.448	0.507	1.13	0.454	1.01
25	0.451	0.507	1.12	0.352	0.78
50	0.162	0.212	1.31	0.205	1.26
75	0.147	0.147	1.00	0.140	0.95
100	0.121	0.136	1.13	0.112	0.93
* Ratio of previous column to the displacement with no FRP.					

Table 12: Estimation of Poisson's ratio from LVDT.

Series	Sample	ε_{v1}	ε_{v2}	ε_{n1}	ε_{n2}	Avg. ε_v	Avg. ε_n	Poisson's Ratio, υ ($\varepsilon_n/\varepsilon_v$)	Poisson's Ratio for each Series
0	1	0.033	0.032	0.009	0.003	0.033	0.006	0.187	0.203
	2	0.022	0.024	0.008	0.002	0.023	0.005	0.220	
1	1	0.036	0.028	0.011	0.007	0.032	0.009	0.271	0.231
	2	0.035	0.036	0.010	0.004	0.036	0.007	0.190	
2	1	0.011	0.034	0.000	0.003	0.022	0.002	0.070	0.079
	2	0.026	0.034	0.002	0.004	0.030	0.003	0.089	

Table 13. P_v-δ bilinear curve-fitting parameters.

	Fitting Parameters versus Normal Loading Levels						
	Parameter	**0%**	**12.5%**	**25%**	**50%**	**75%**	**100%**
Series 0	a_0 [lb/in]	86882.6	84880.95	74500.59	134515.2	158917.8	412582.3
	b_0 [lb/in]	---	3149.07	23708.07	26968.75	---	---
	b_1 [lb]	---	10298.22	23708.07	14196.13	---	---
	δ_{ult} [in]	---	0.448	0.450	0.164	---	---
Series I	a_0 [lb/in]	59166.74	77406.06	78759.26	113196	120606.7	301114.7
	b_0 [lb/in]	---	0.00	13997.83	0.00	---	---
	b_1 [lb]	---	12772	10491.35	16329.95	---	---
	δ_{ult} [in]	---	0.500	0.368	0.212	---	---
Series II	a_0 [lb/in]	85266.3	117348.6	83184.94	93851.32	143233	432572.3
	b_0 [lb/in]	---	1442.84	16934.28	0.00	19773.95	---
	b_1 [lb]	---	12031.01	11964.87	18432.4	19773.95	---
	δ_{ult} [in]	---	0.454	0.352	0.205	0.140	---

Table 14. Mohr-Coulomb and Generalized Failure Criteria parameters for brick triplets.

	Fitting Parameters versus Series			
	Parameter	**Series 0 (without FRP)**	**Series I (one-side FRP)**	**Series II (two-side FRP)**
Mohr-Coulomb Model	μ	0.795	0.848	0.621
	σ_v^0 [psi]	54.95	79.60	120.2
Generalized Model	a_1 [psi]	47.000	79.839	119.80
	a_2	1.6448	1.4670	1.3963
	a_3 [psi^{-1}]	-3.6573×10^{-3}	-3.8965×10^{-3}	-3.5141×10^{-3}
	a_4 [psi^{-2}]	3.8104×10^{-6}	4.7565×10^{-6}	3.8618×10^{-6}
	a_5 [psi^{-3}]	-1.5125×10^{-9}	-2.1537×10^{-9}	-1.5372×10^{-9}

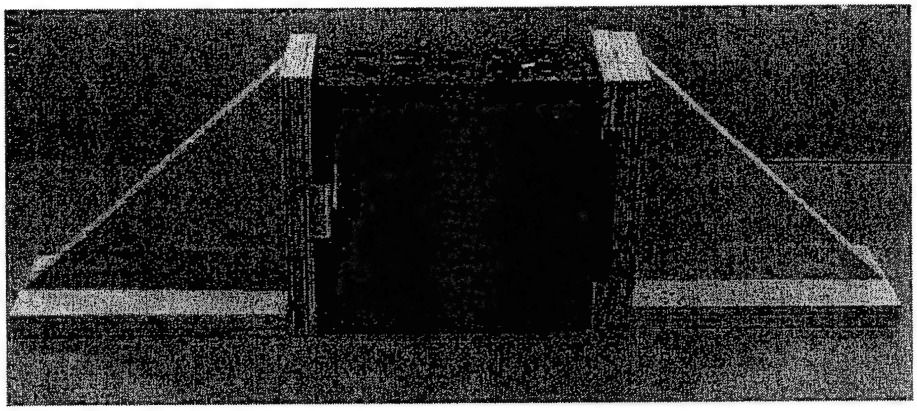

Figure 1. Construction of triplet samples.

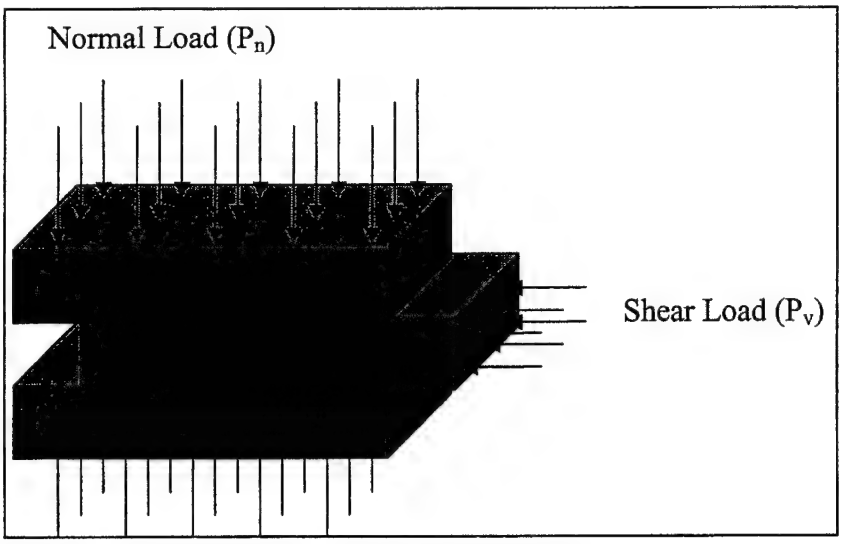

Figure 2. Triplet test under normal and shear loads.

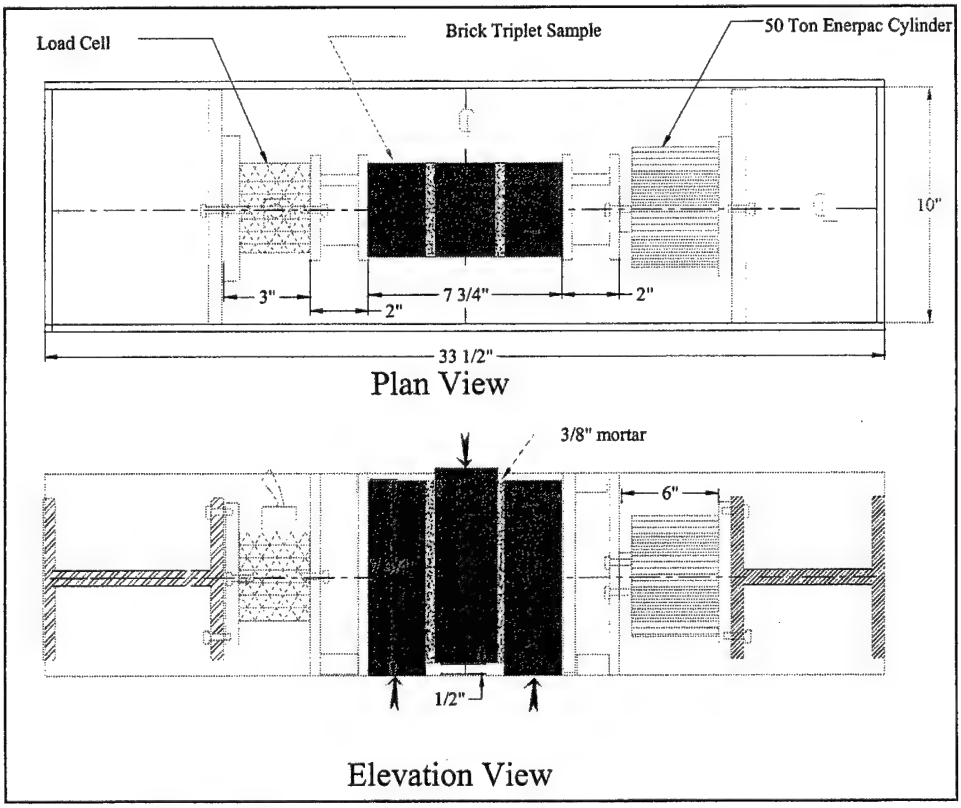

Figure 3. Biaxial loading test frame.

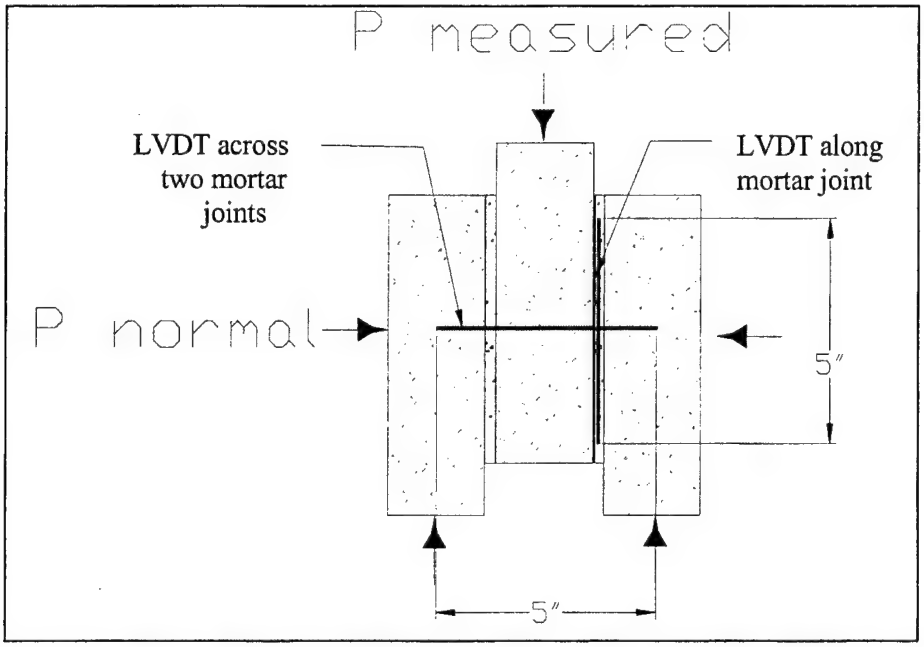

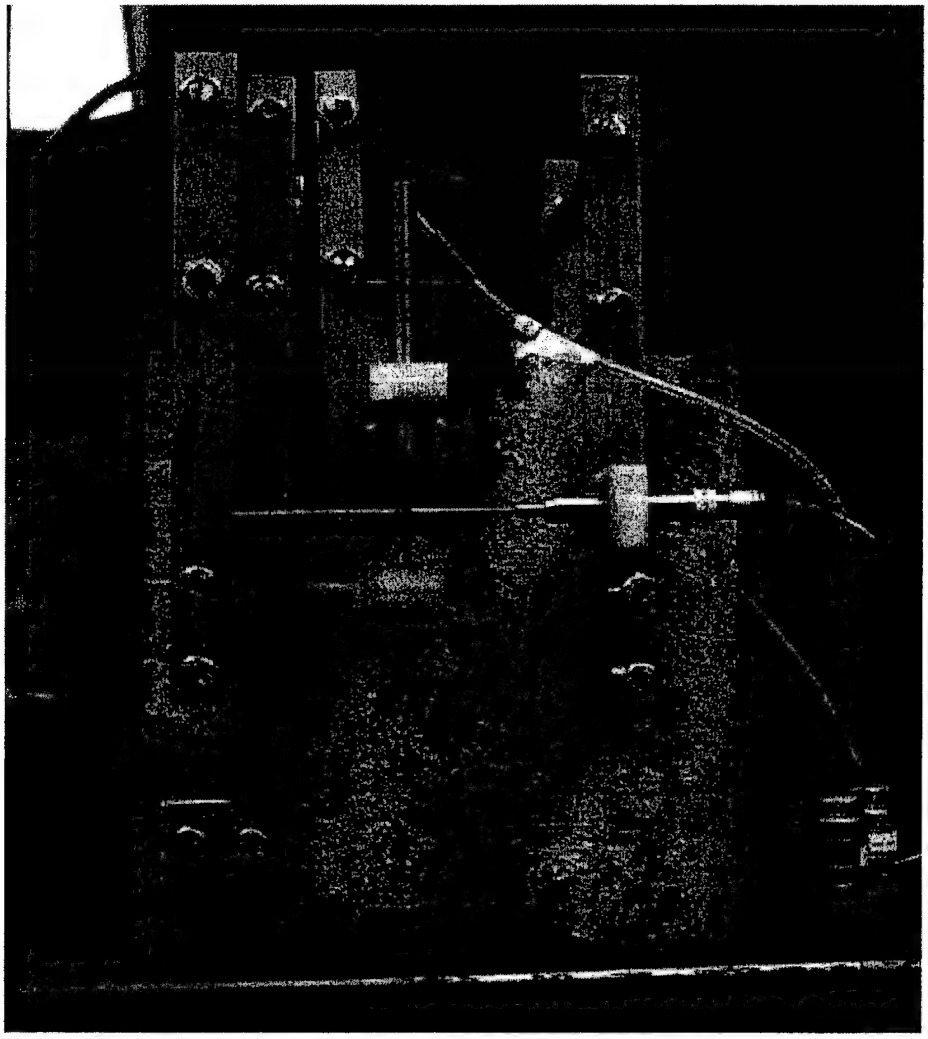

Figure 4. Schematic (top) and photo (bottom) of triplet test with LVDT.

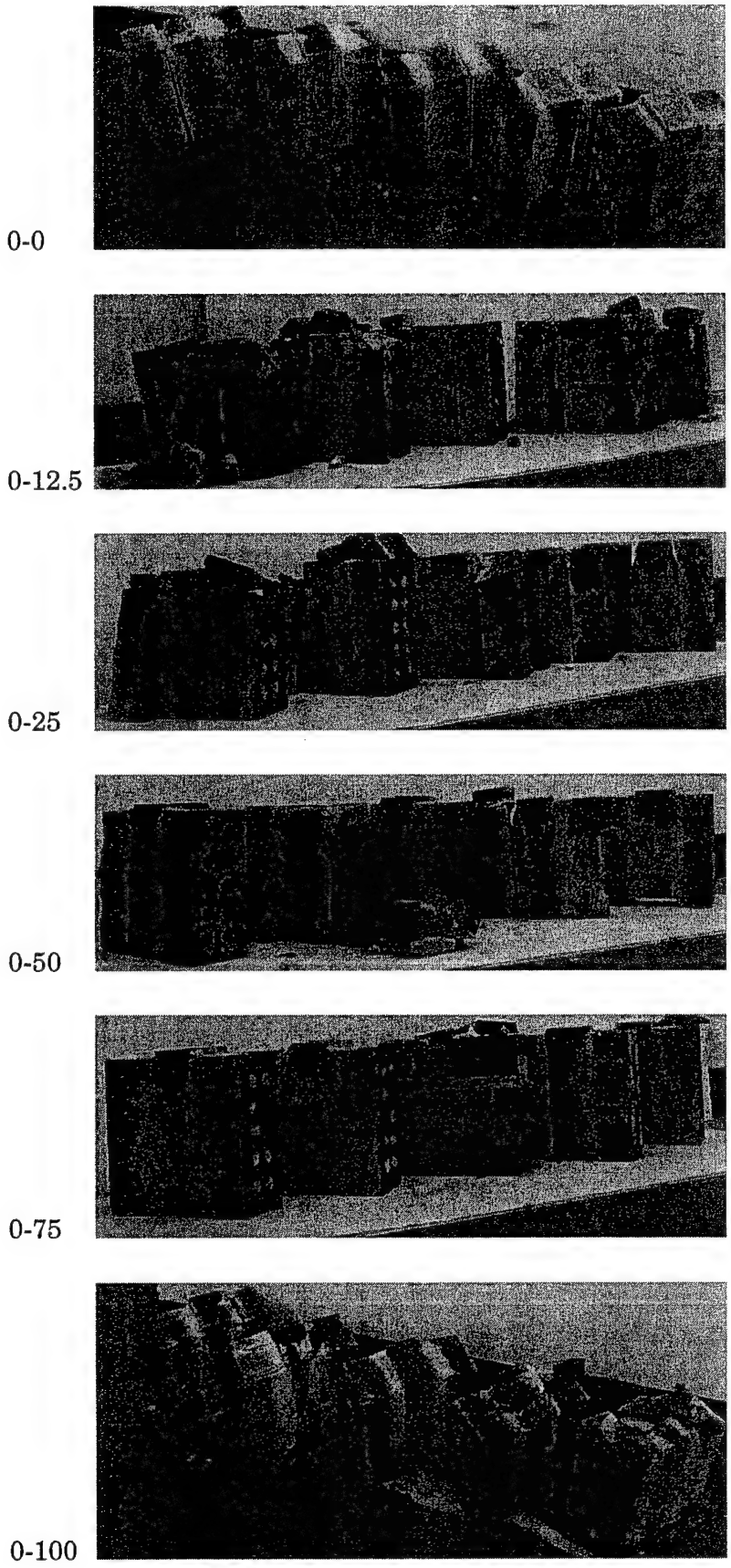

Figure 5. Modes of failure for Series 0.

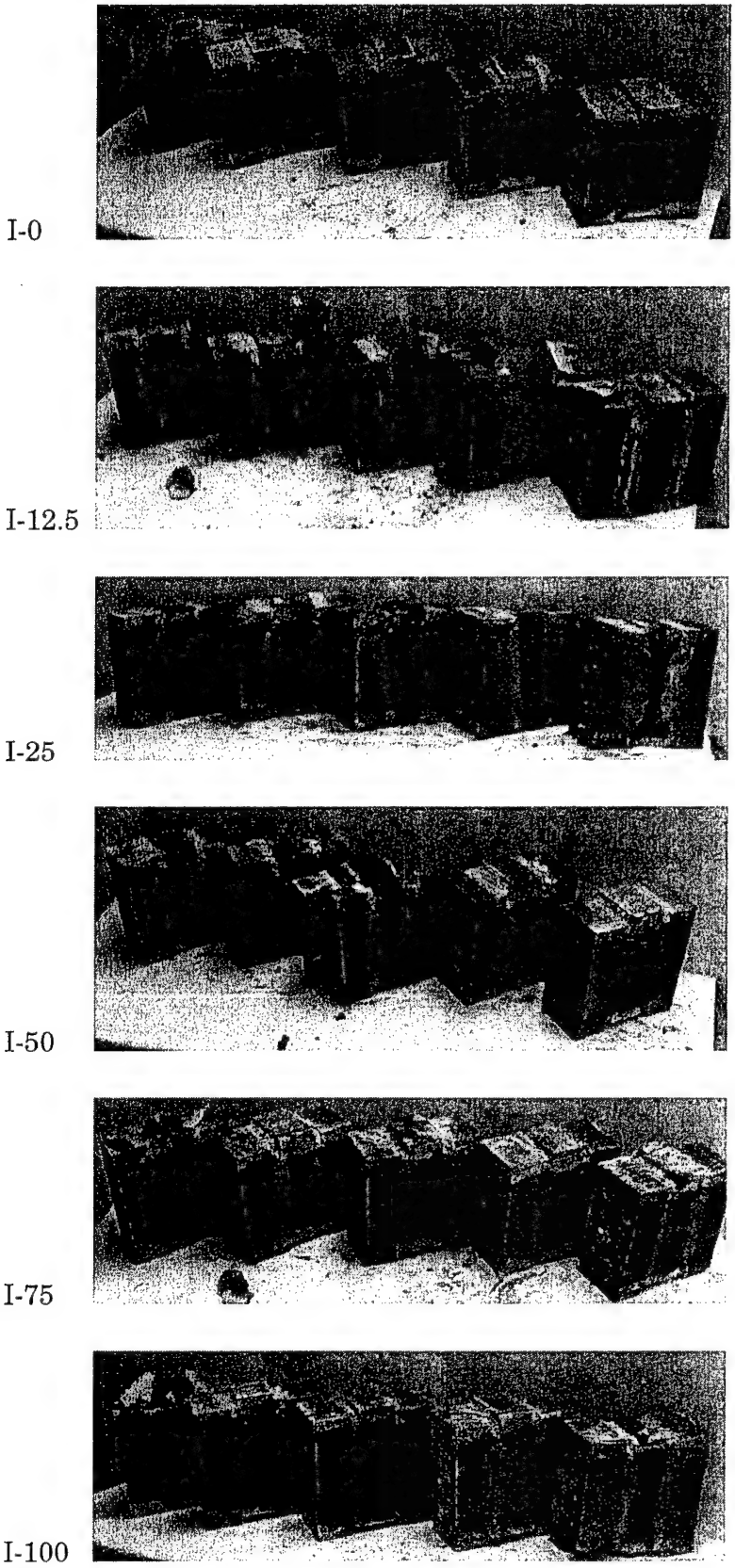

Figure 6. Modes of failure for Series I.

II-0

II-12.5

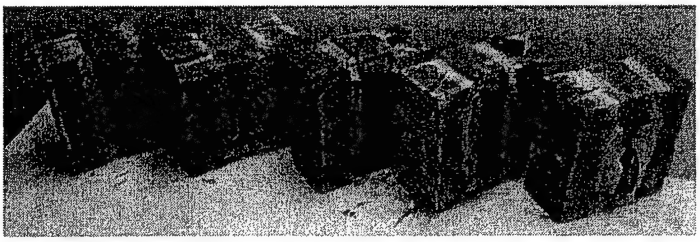

II-25

II-50

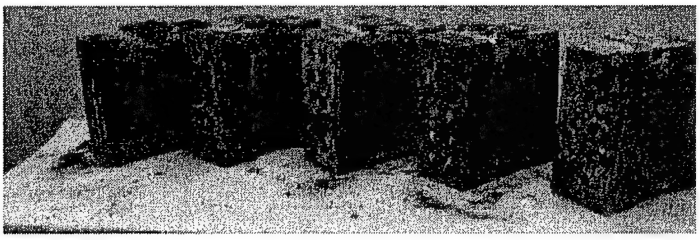

II-75

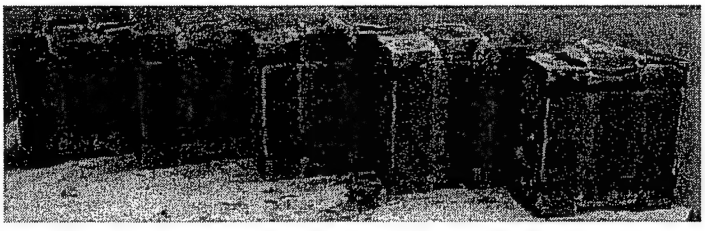

II-100

Figure 7. Modes of failure for Series II.

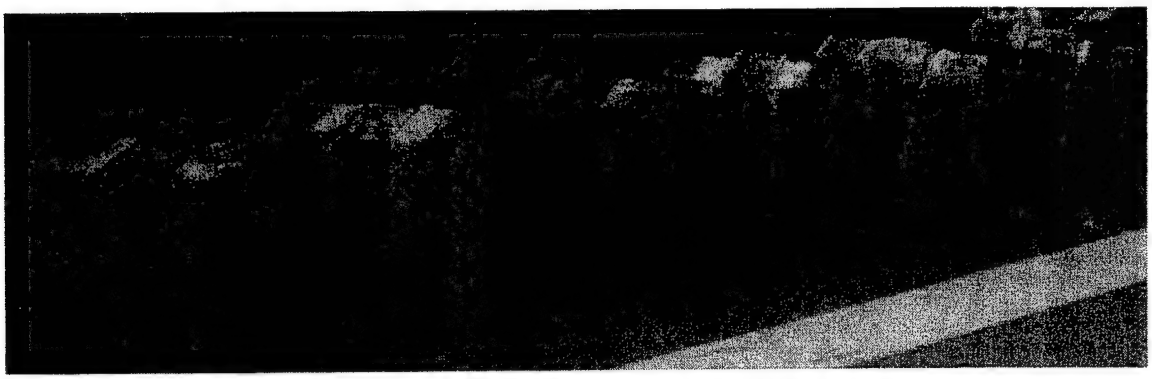

Figure 8. Modes of failure for Series 0, I, and II for samples with LVDTs.

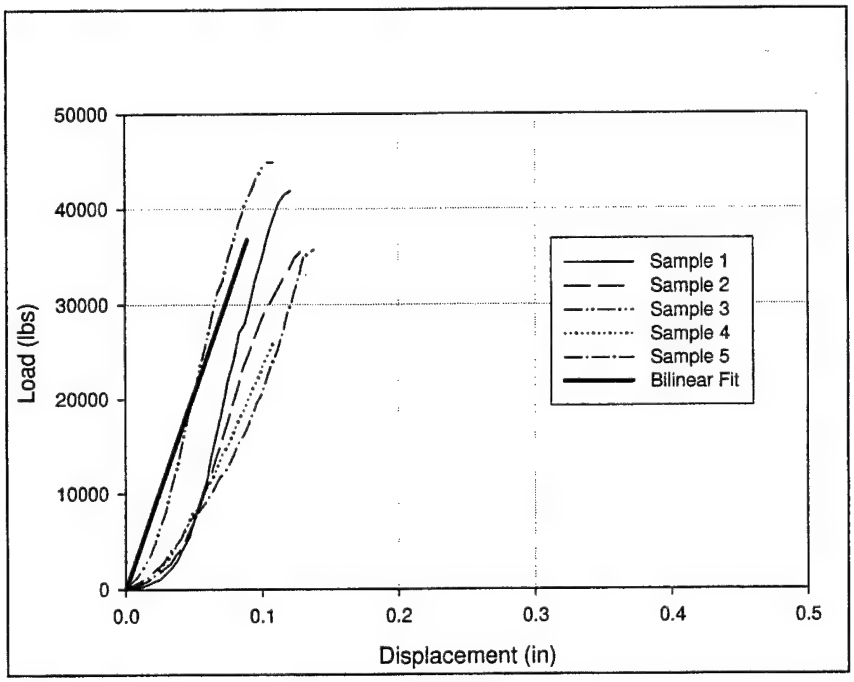

Figure 9. Load-displacement curves of 0-100 group.

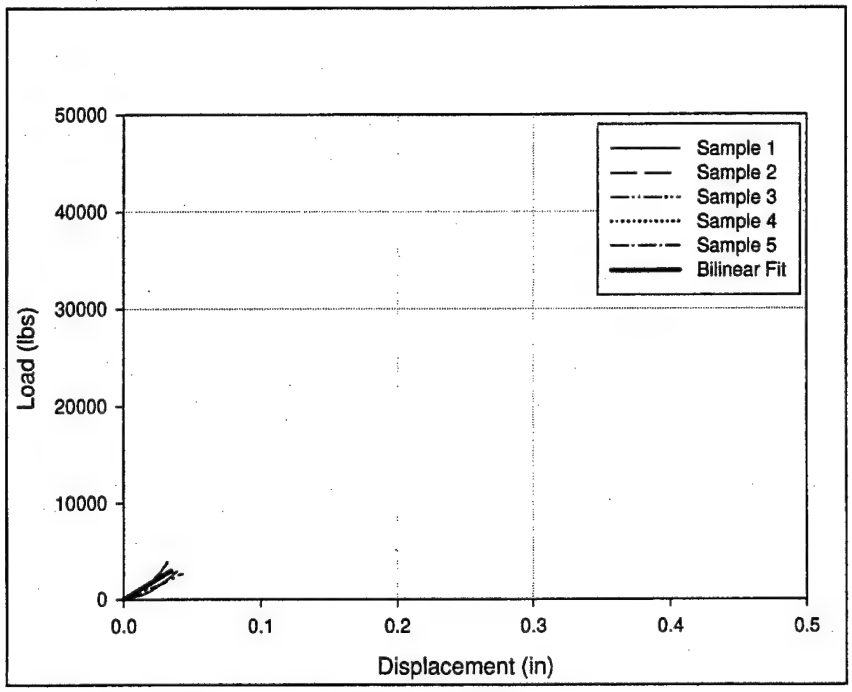

Figure 10. Load-displacement curves of 0-0 group.

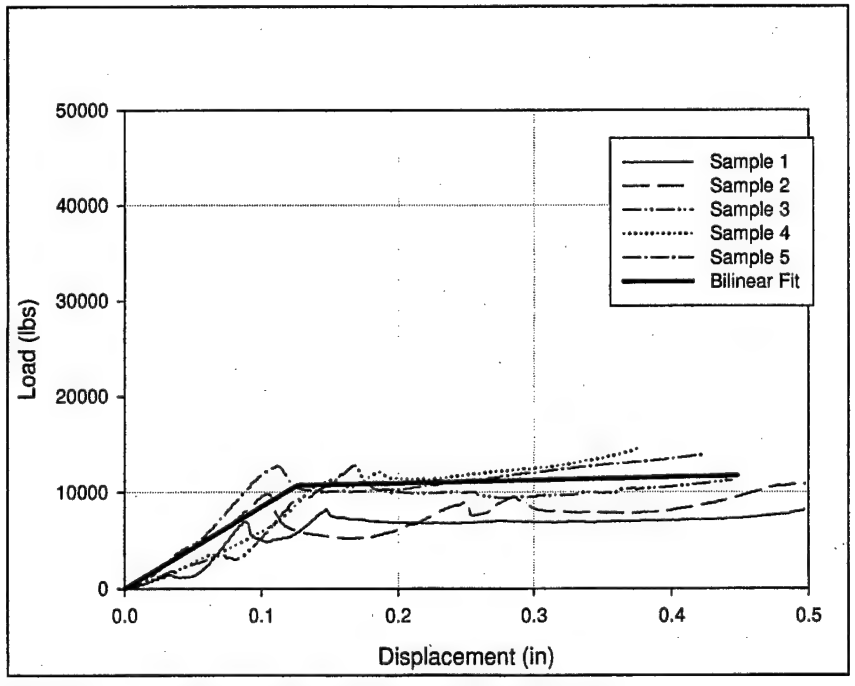

Figure 11. Load-displacement curves of 0-12.5 group.

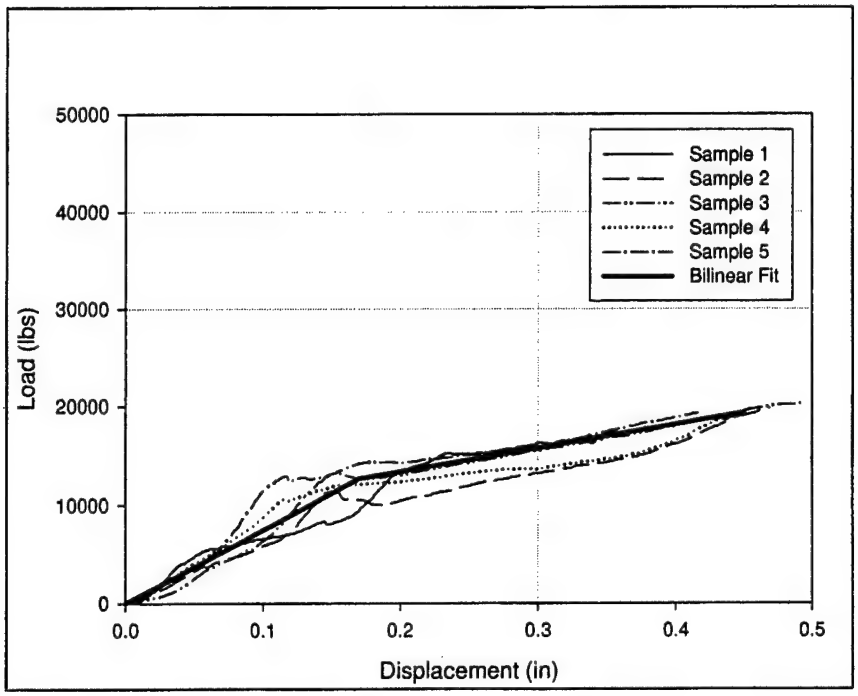

Figure 12. Load-displacement curves of 0-25 group.

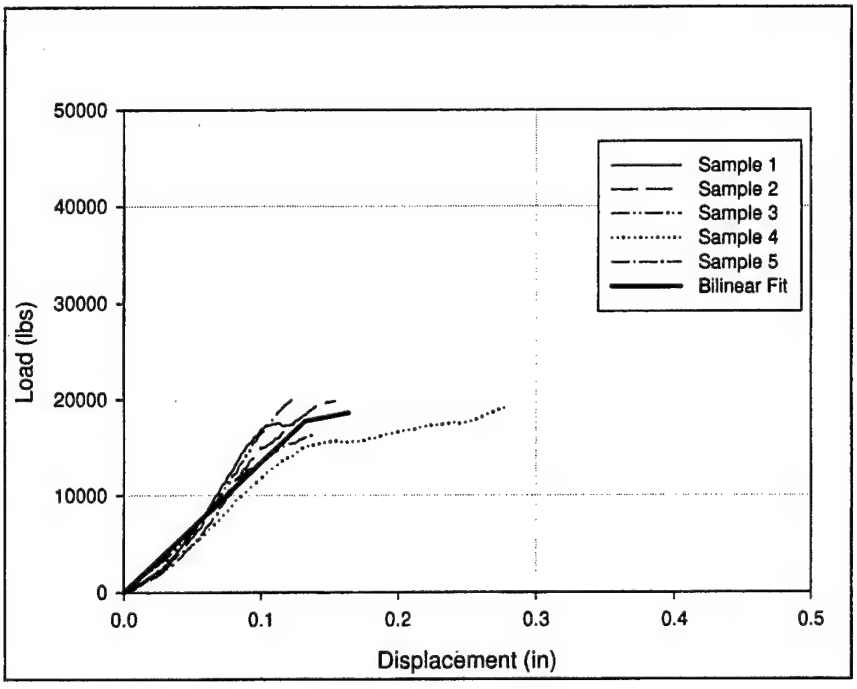

Figure 13. Load-displacement curves of 0-50 group.

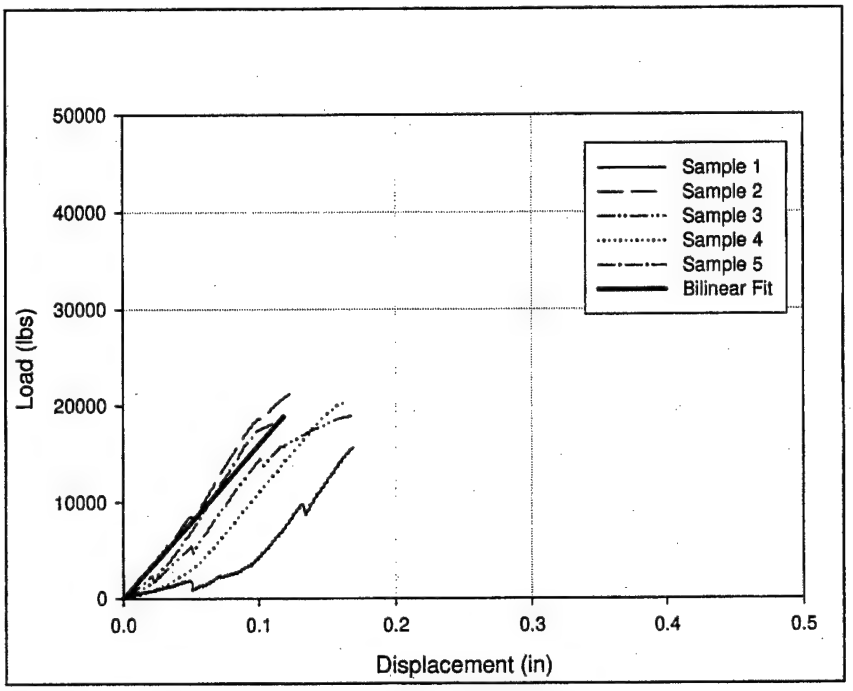

Figure 14. Load-displacement curves of 0-75 Group.

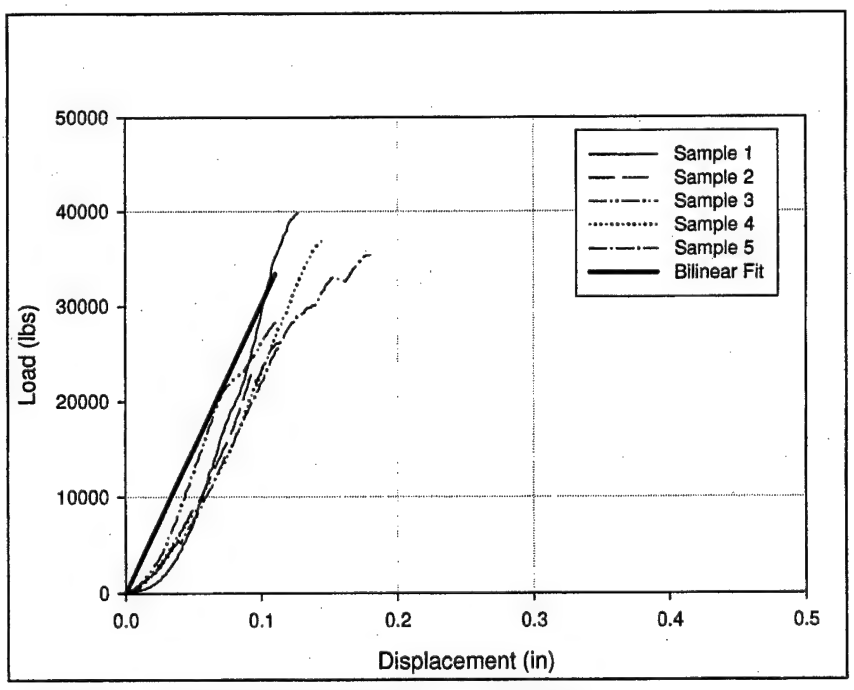

Figure 15. Load-displacement curves of I-100 group.

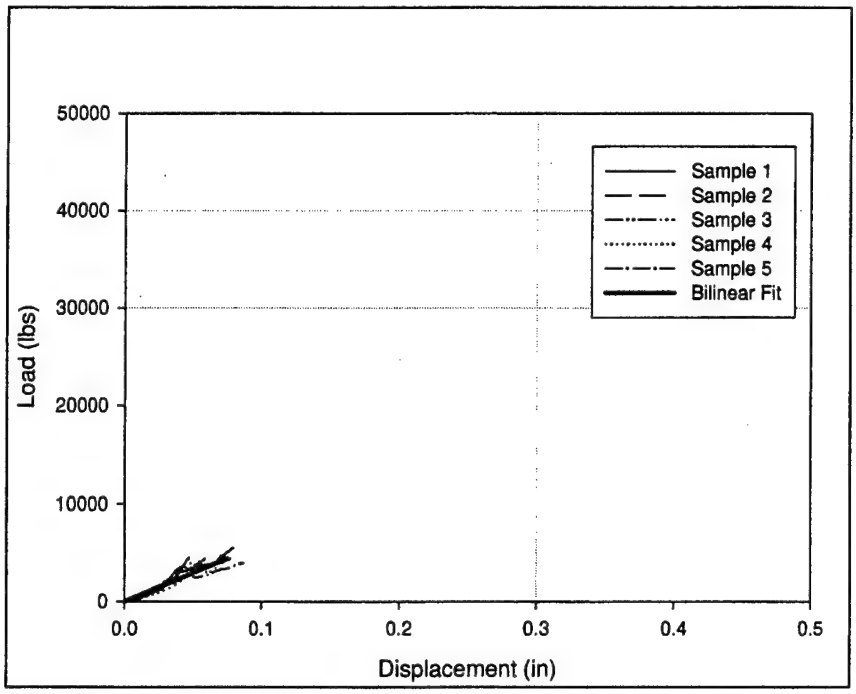

Figure 16. Load-displacement curves of I-0 group.

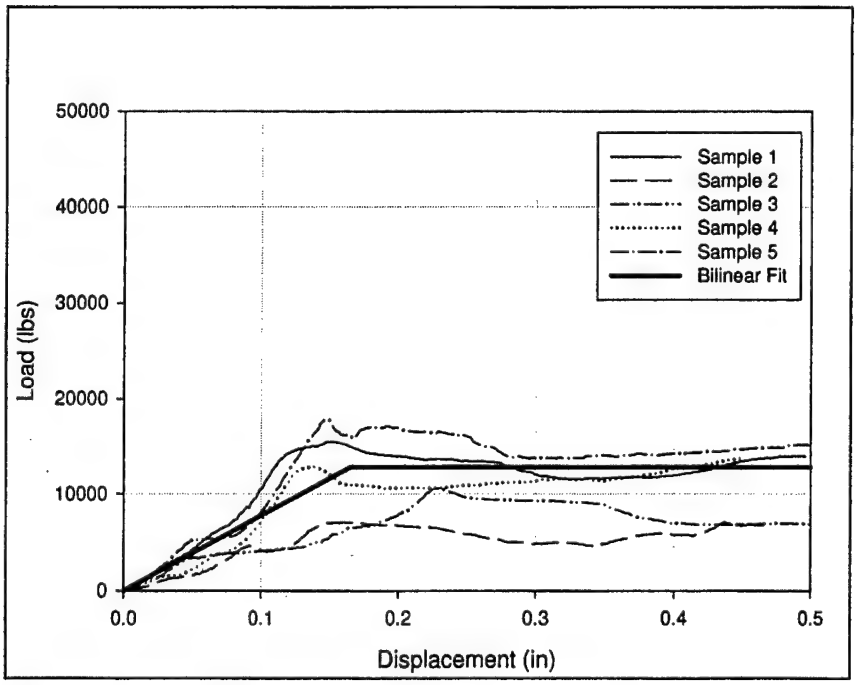

Figure 17. Load-displacement curves of I-12.5 group.

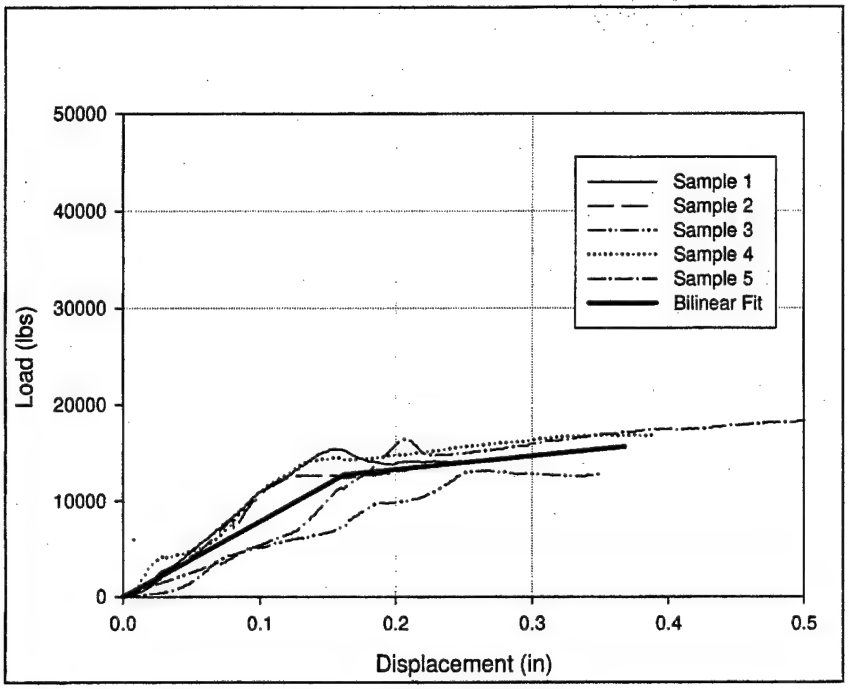

Figure 18. Load-displacement curves of I-25 group.

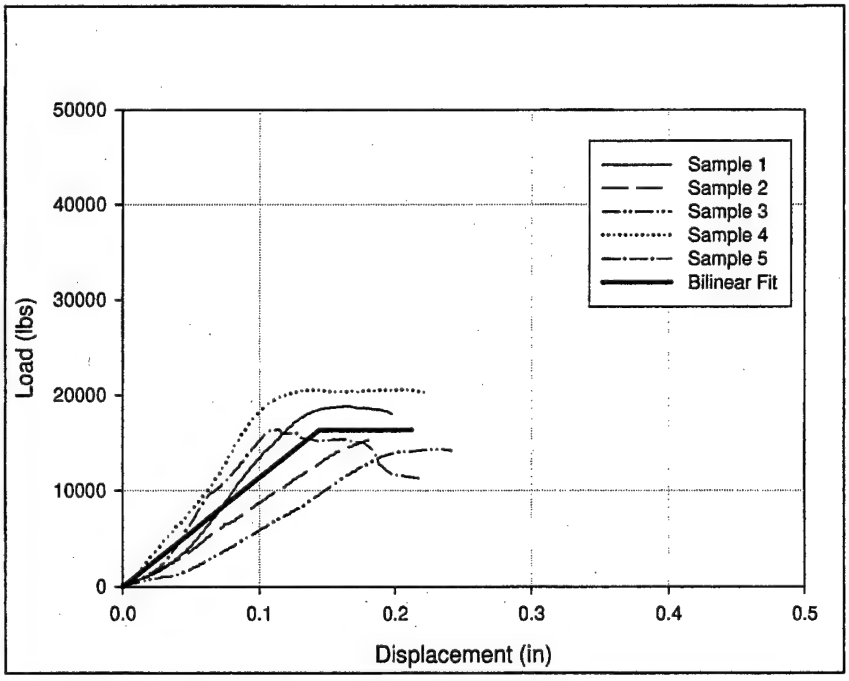

Figure 19. Load-displacement curves of I-50 group.

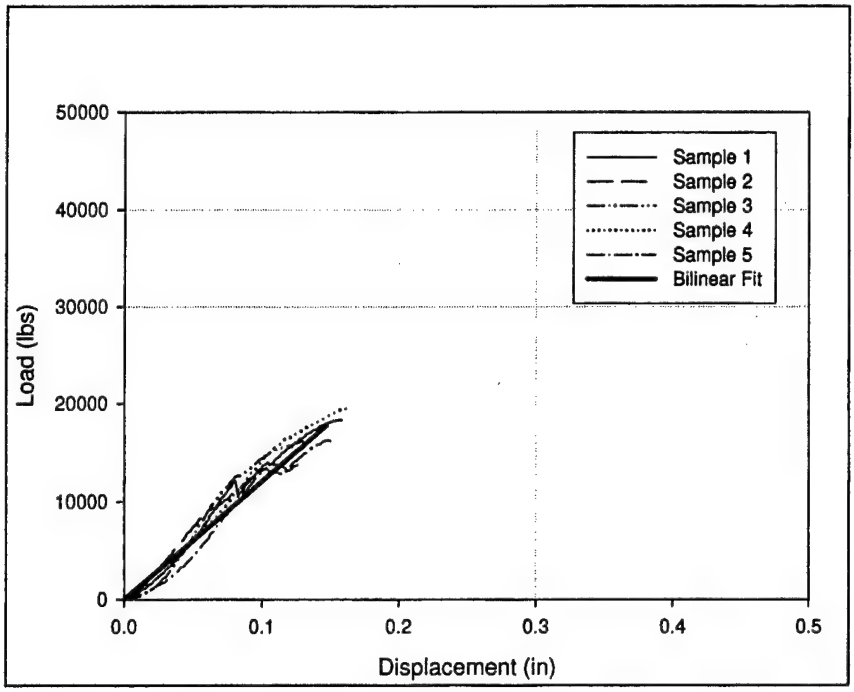

Figure 20. Load-displacement curves of I-75 group.

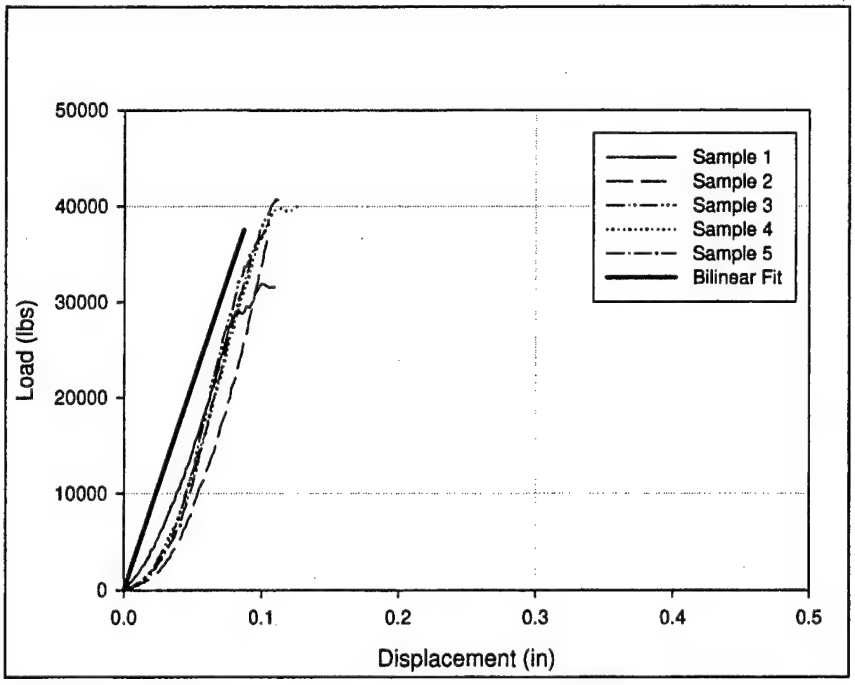

Figure 21. Load-displacement curves of II-100 Group.

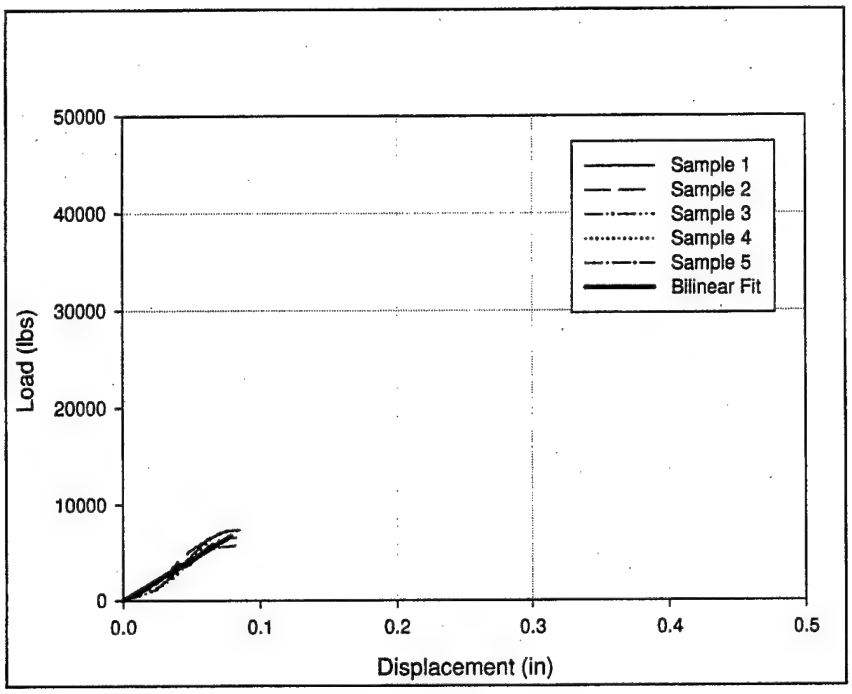

Figure 22. Load-displacement curves of II-0 group.

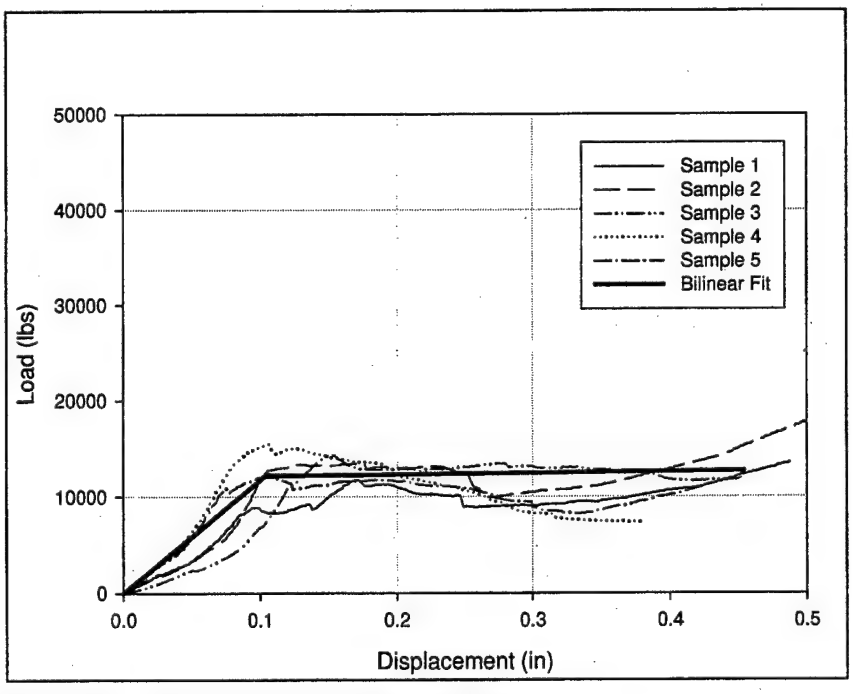

Figure 23. Load-displacement curves of II-12.5 group.

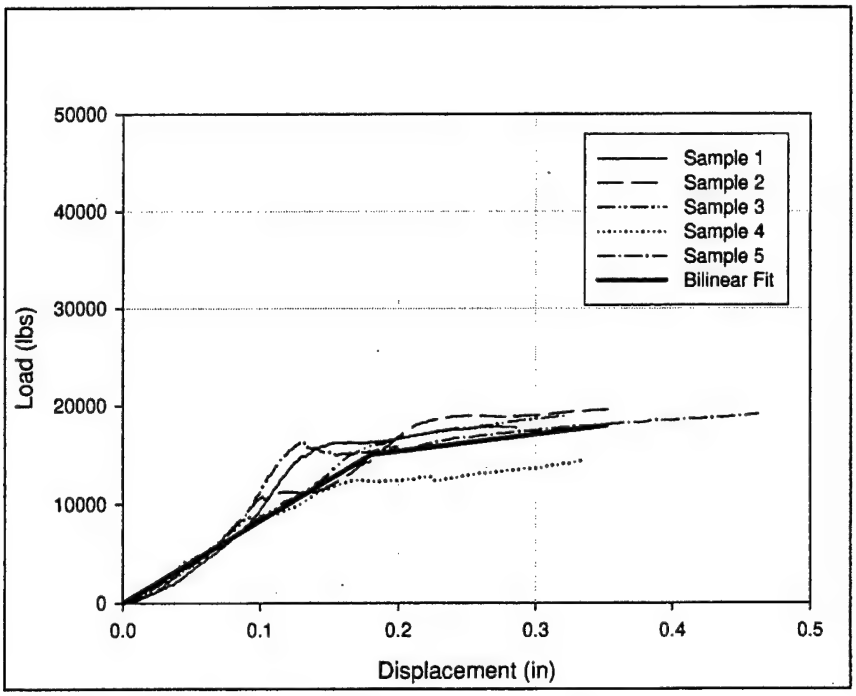

Figure 24. Load-displacement curves of II-25 group.

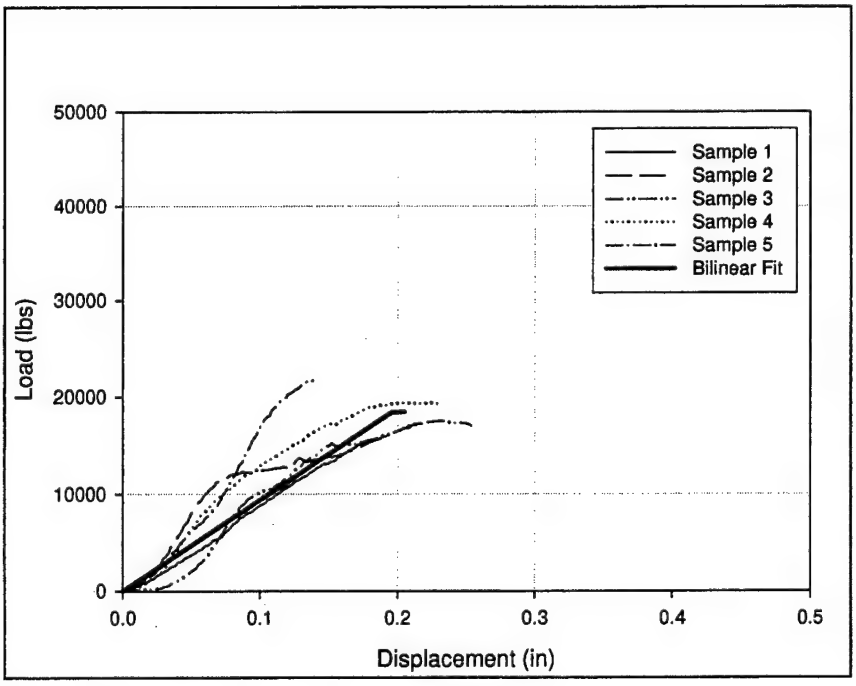

Figure 25. Load-displacement curves of II-50 group.

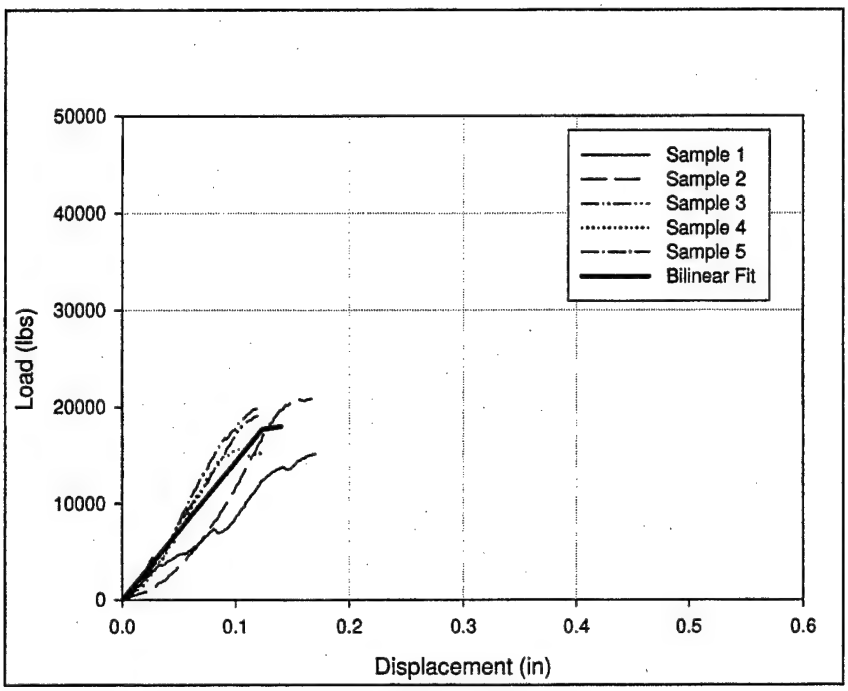

Figure 26. Load-displacement curves of II-75 group.

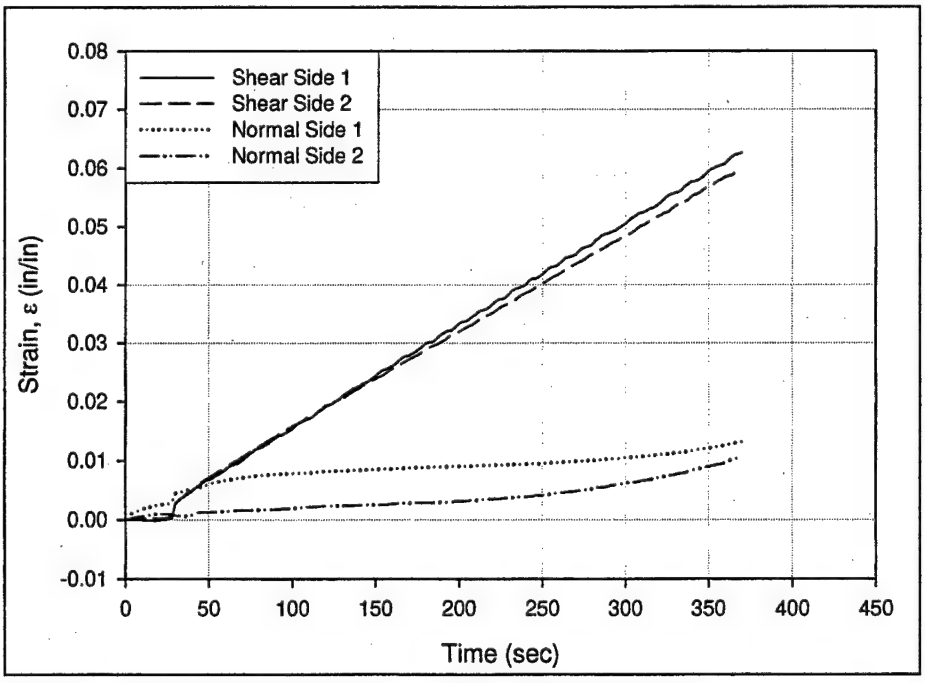

Figure 27. Normal and shear strain vs time of 0-LVDT, Sample 1.

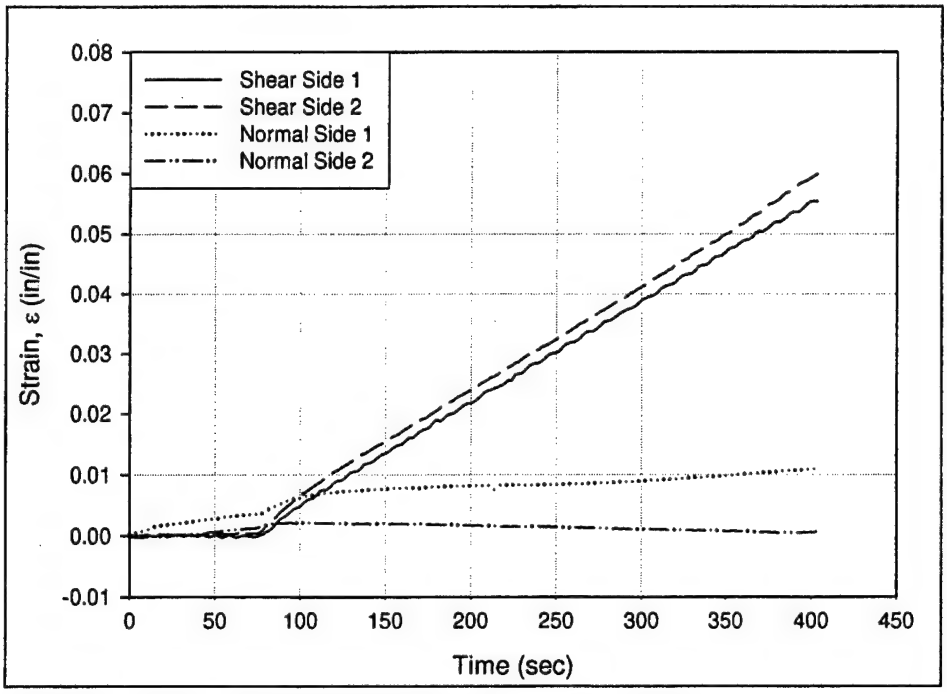

Figure 28. Normal and shear strain vs time of 0-LVDT, Sample 2.

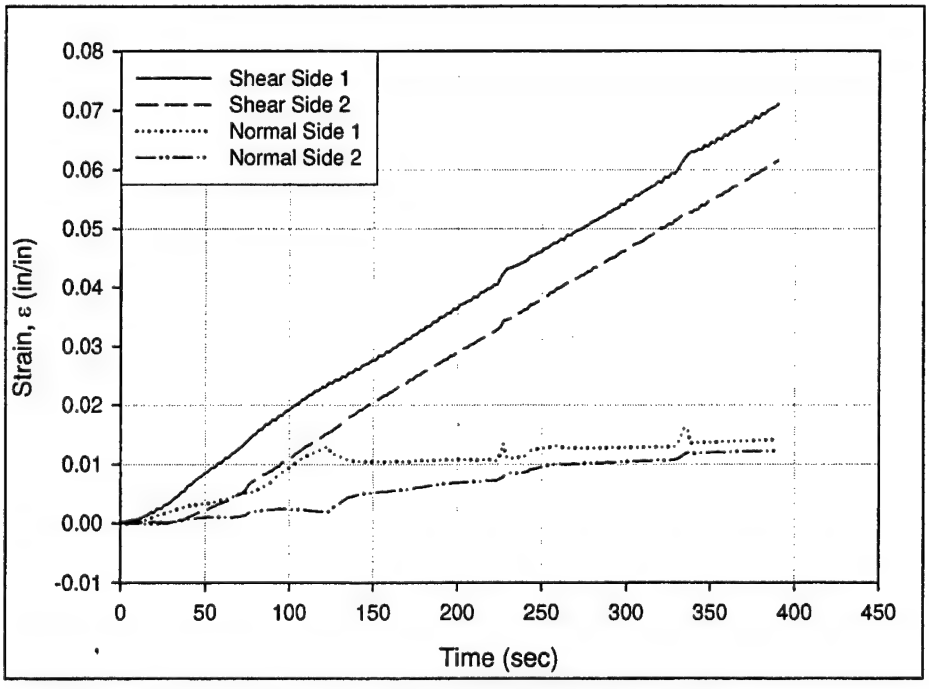

Figure 29. Normal and shear strain vs time of I-LVDT, Sample 1.

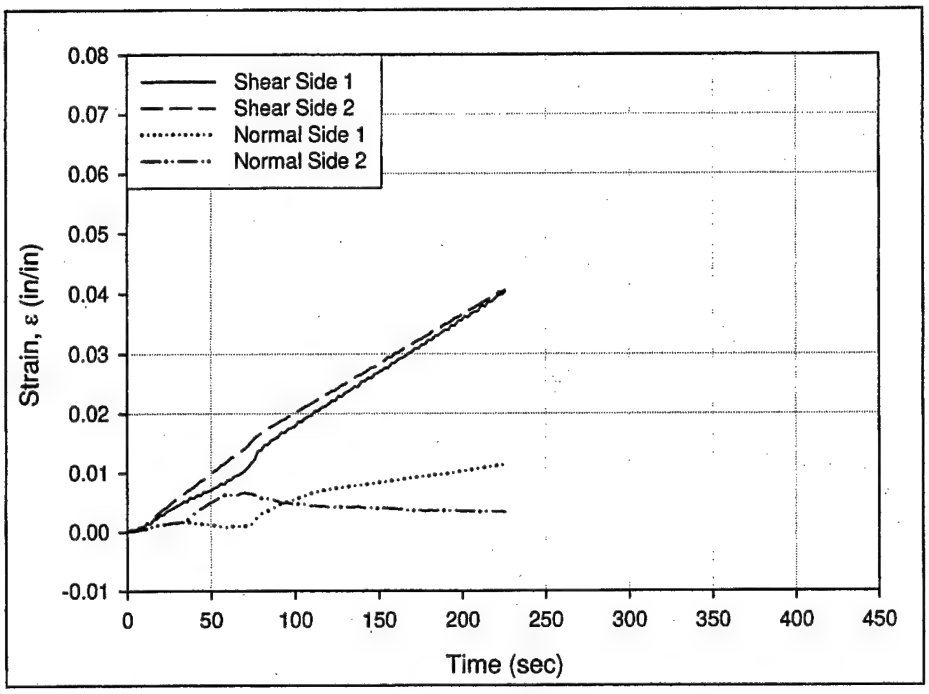

Figure 30. Normal and shear strain vs time of I-LVDT, Sample 2.

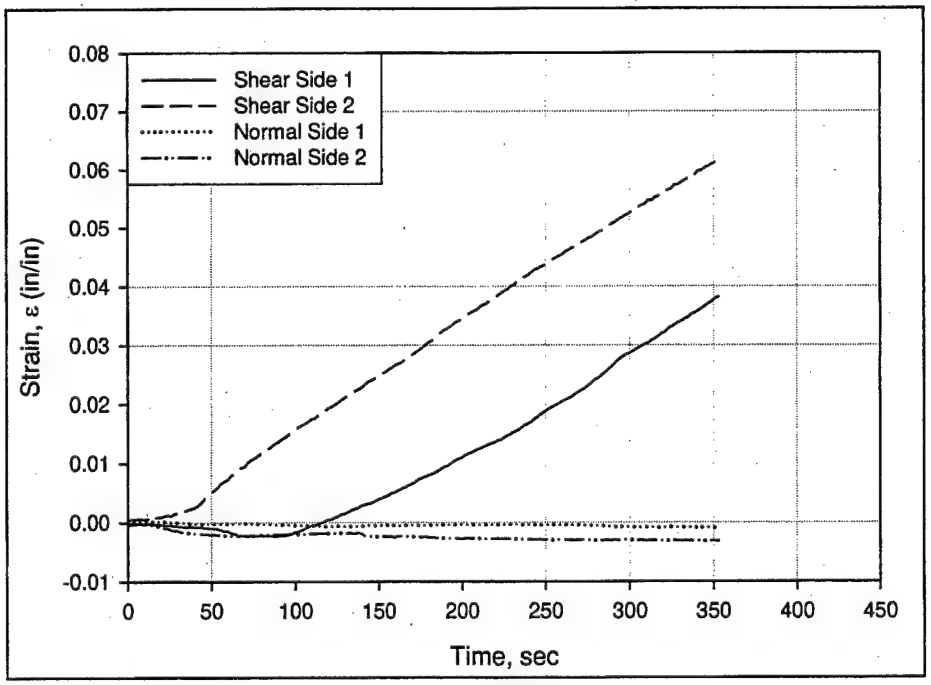

Figure 31. Normal and shear strain vs time of II-LVDT, Sample 1.

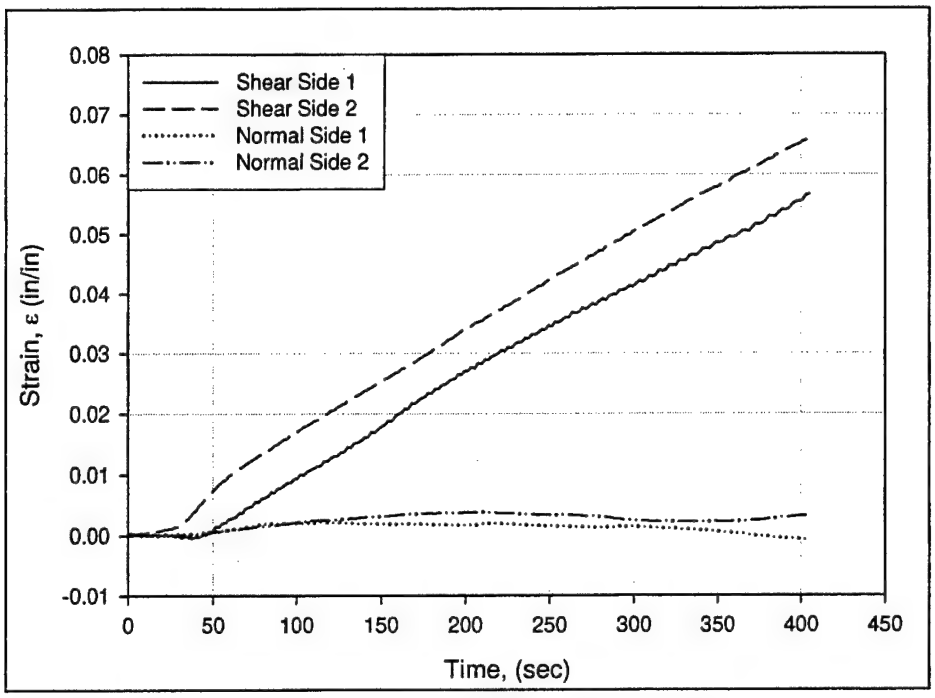

Figure 32. Normal and shear strain vs time of II-LVDT, Sample 2.

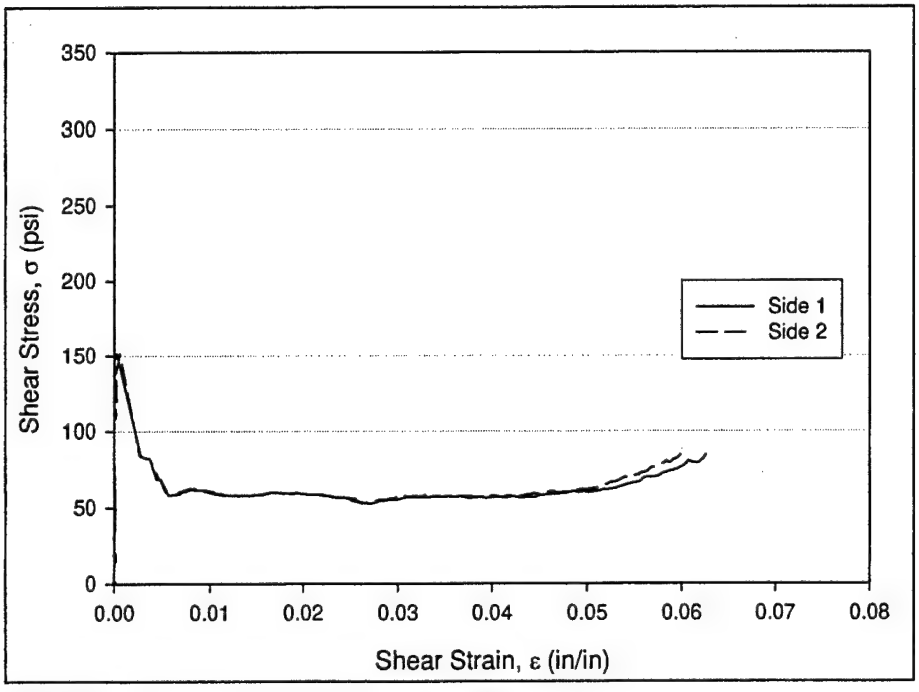

Figure 33. Stress-Strain Behavior of 0-LVDT, Sample 1.

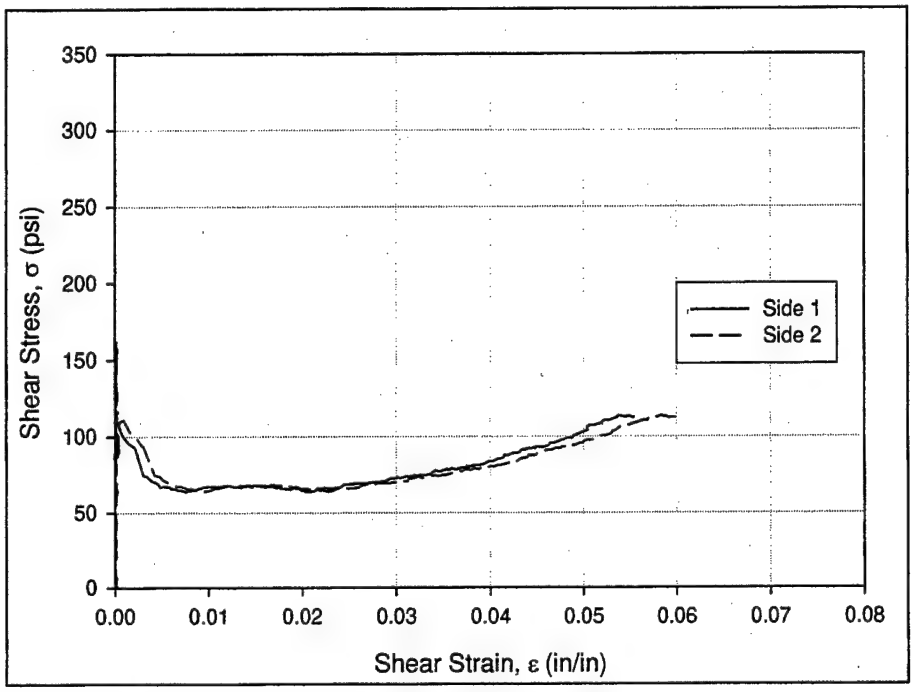

Figure 34. Stress-strain behavior of 0-LVDT, Sample 2.

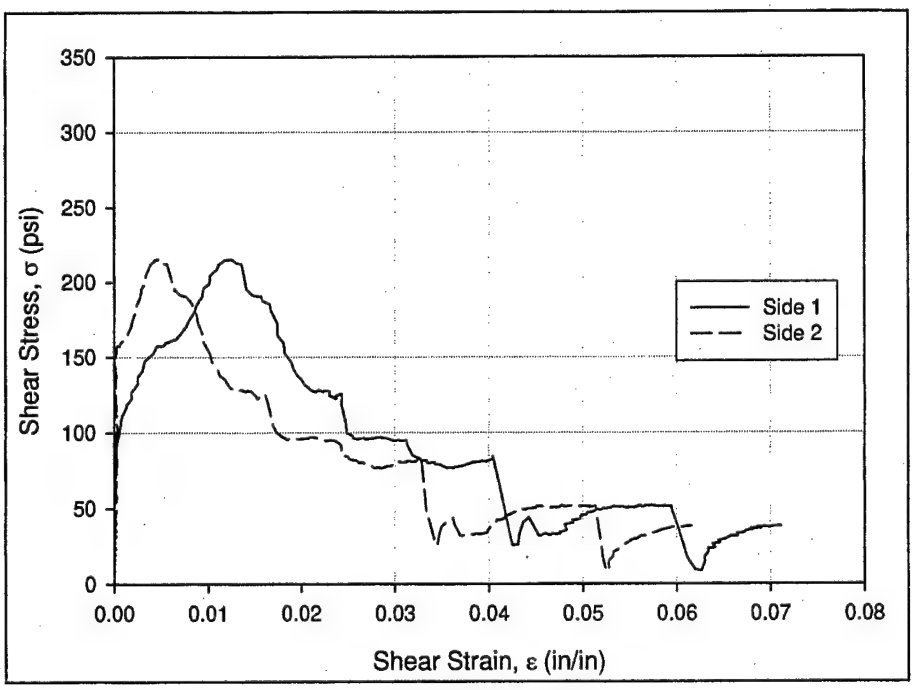

Figure 35. Stress-strain behavior of I-LVDT, Sample 1.

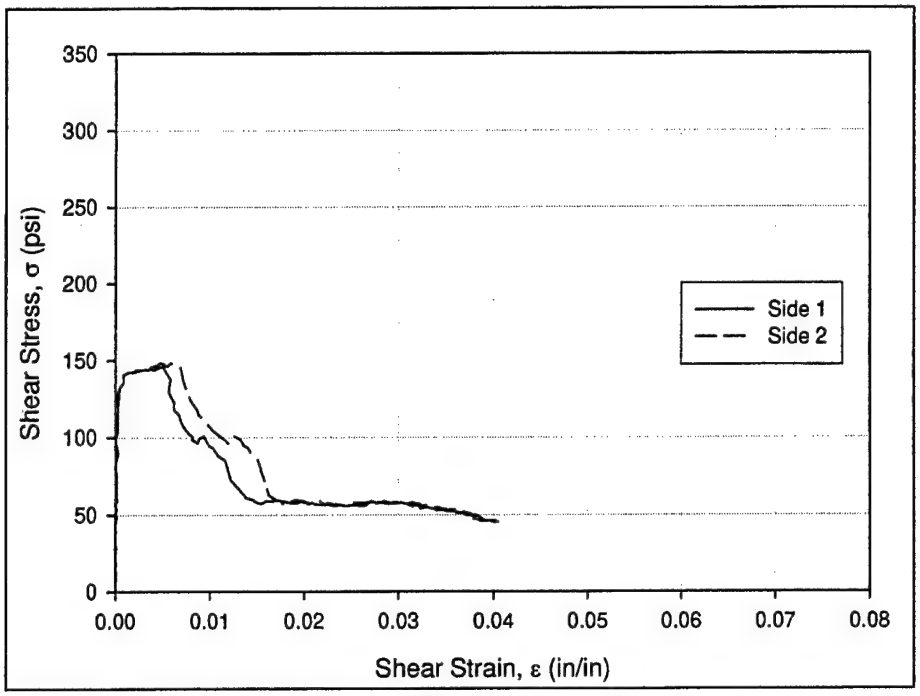

Figure 36. Stress-strain behavior of I-LVDT, Sample 2.

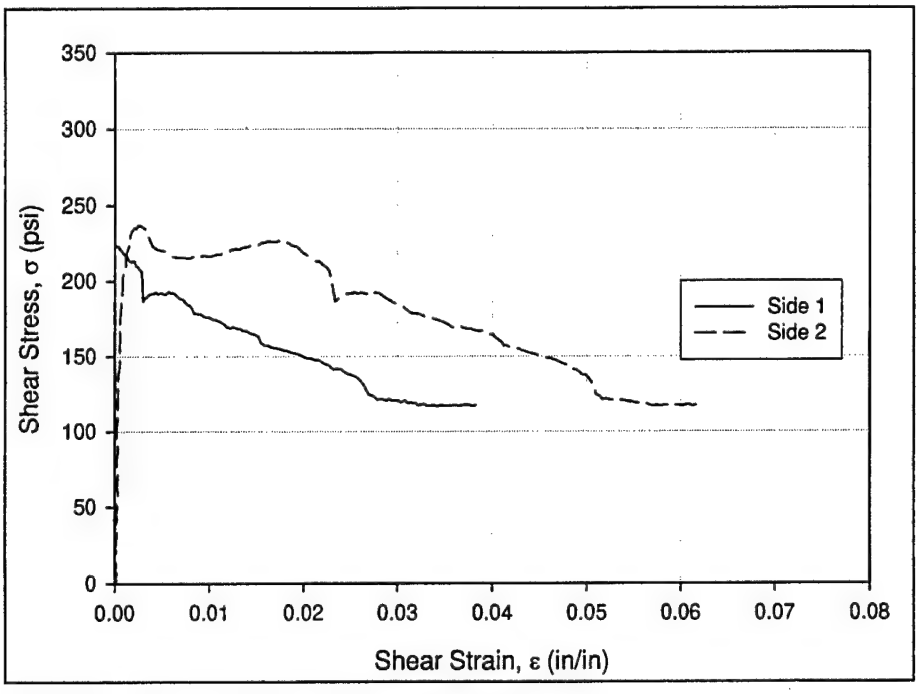

Figure 37. Stress-strain behavior of II-LVDT, Sample 1.

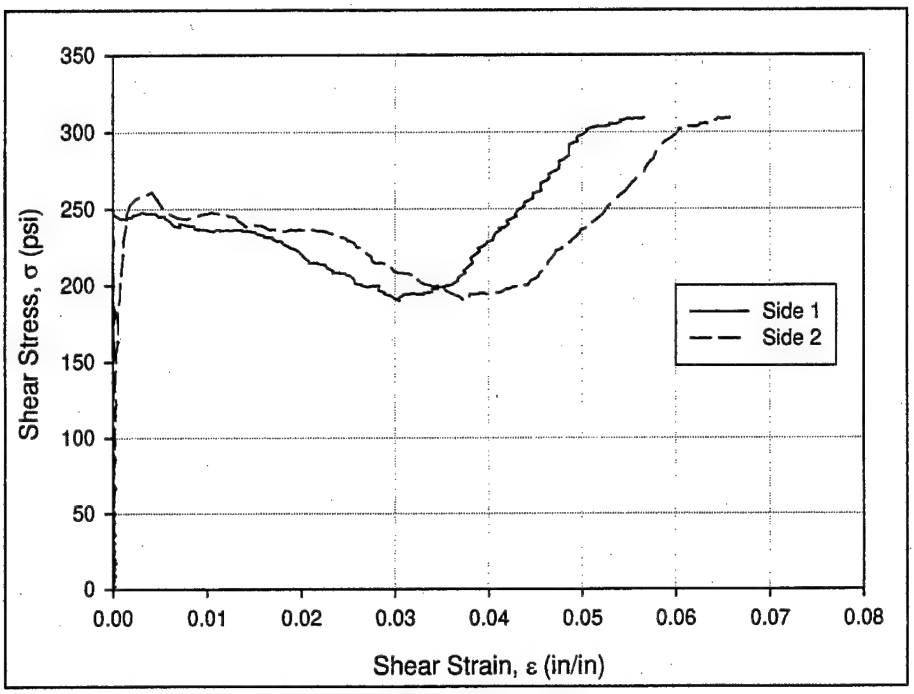

Figure 38. Stress-strain behavior of II-LVDT, Sample #2.

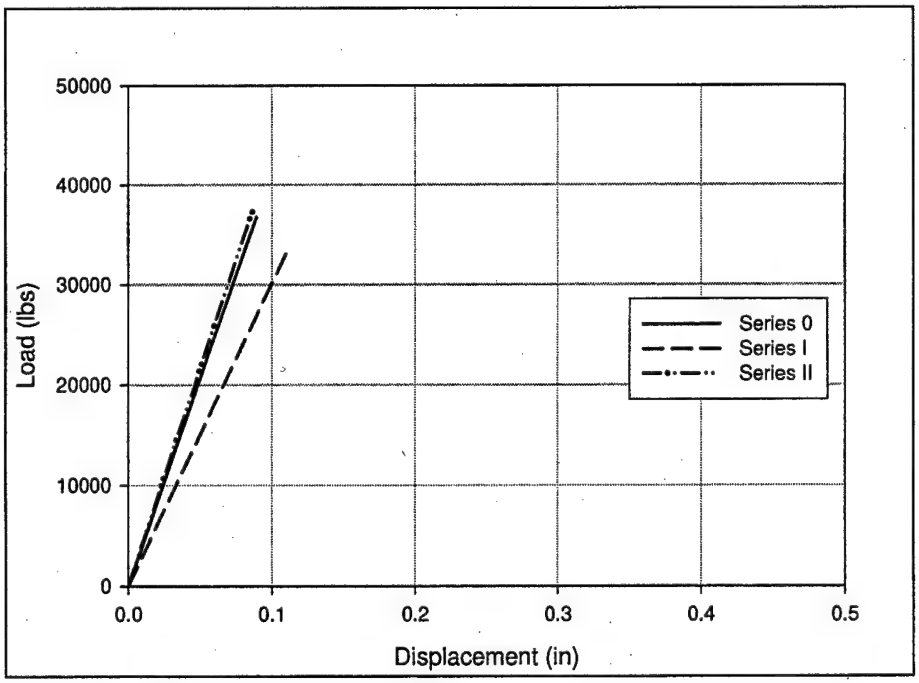

Figure 39. Idealized bilinear curve fit for Series 0, I, II at 100% normal load.

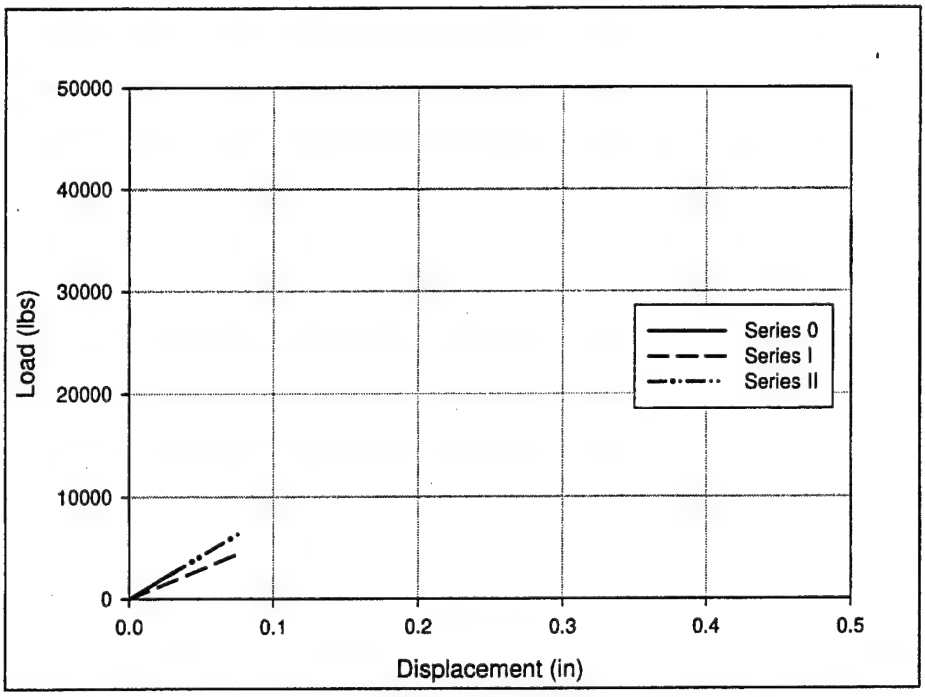

Figure 40. Idealized bilinear curve fit for series 0, I, II at 0% normal load.

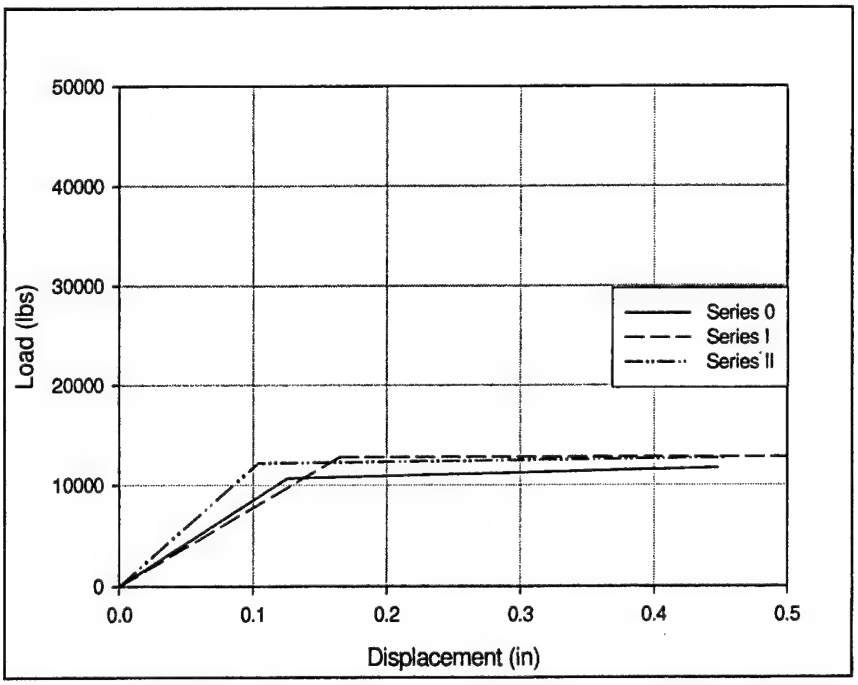

Figure 41. Idealized bilinear curve fit for Series 0, I, II at 12.5% normal load.

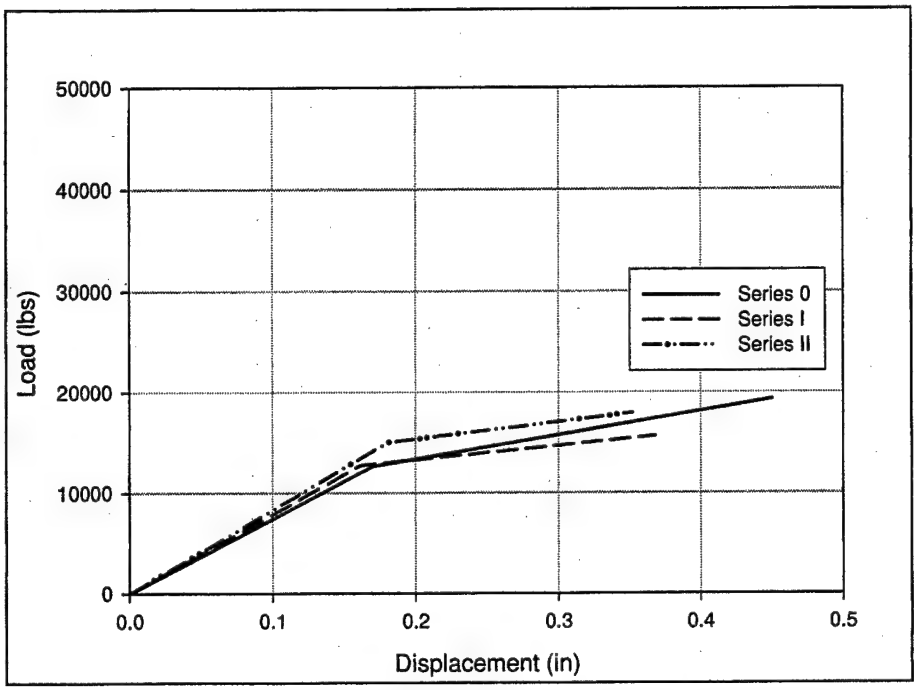

Figure 42. Idealized bilinear curve fit for Series 0, I, II at 25% normal load.

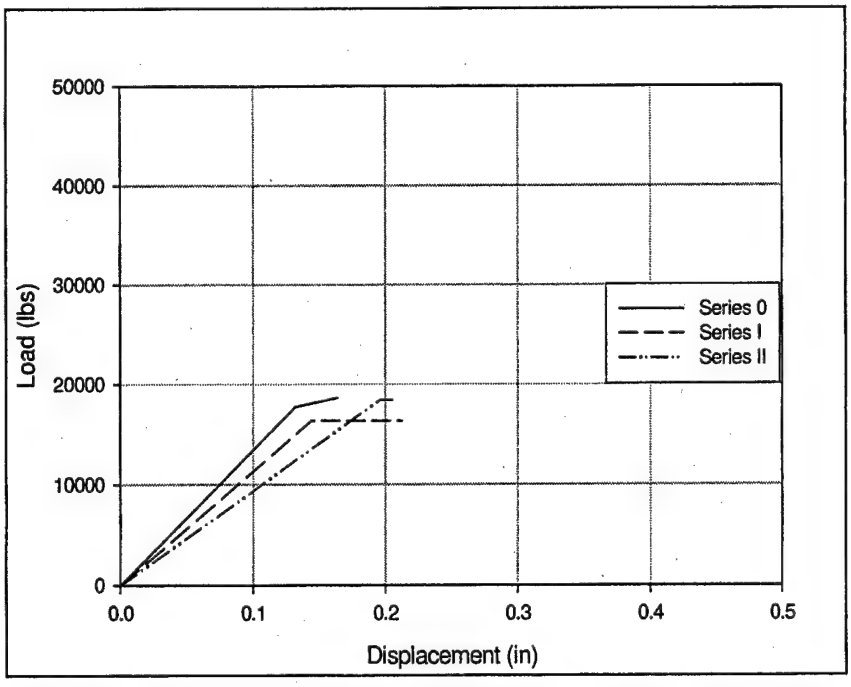

Figure 43. Idealized bilinear curve fit for Series 0, I, II at 50% normal load.

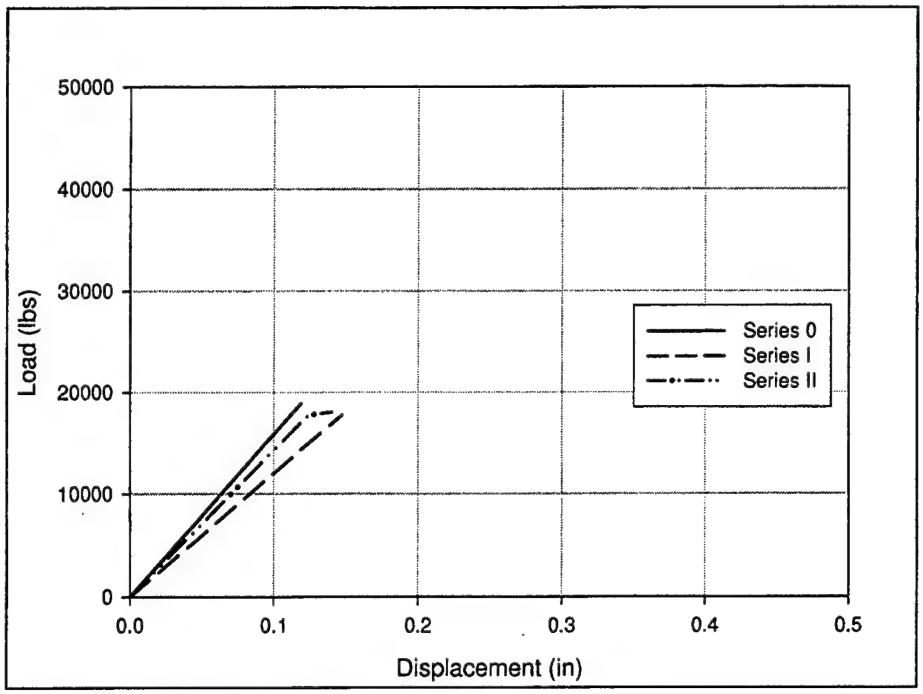

Figure 44. Idealized bilinear curve fit for Series 0, I, II at 75% normal load.

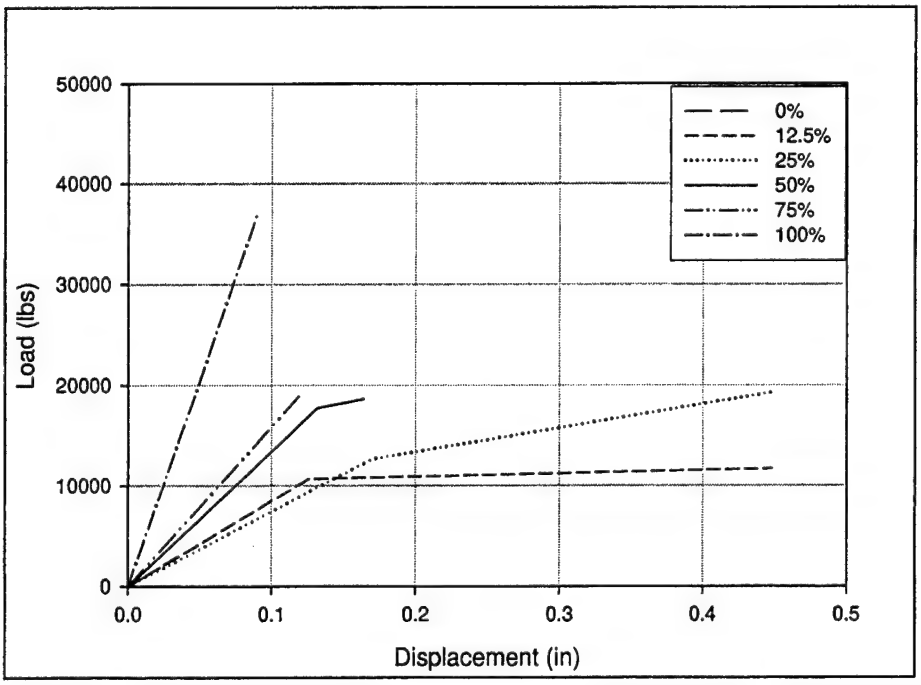

Figure 45. Idealized bilinear curve fit for Series 0 from 0% through 100% normal load.

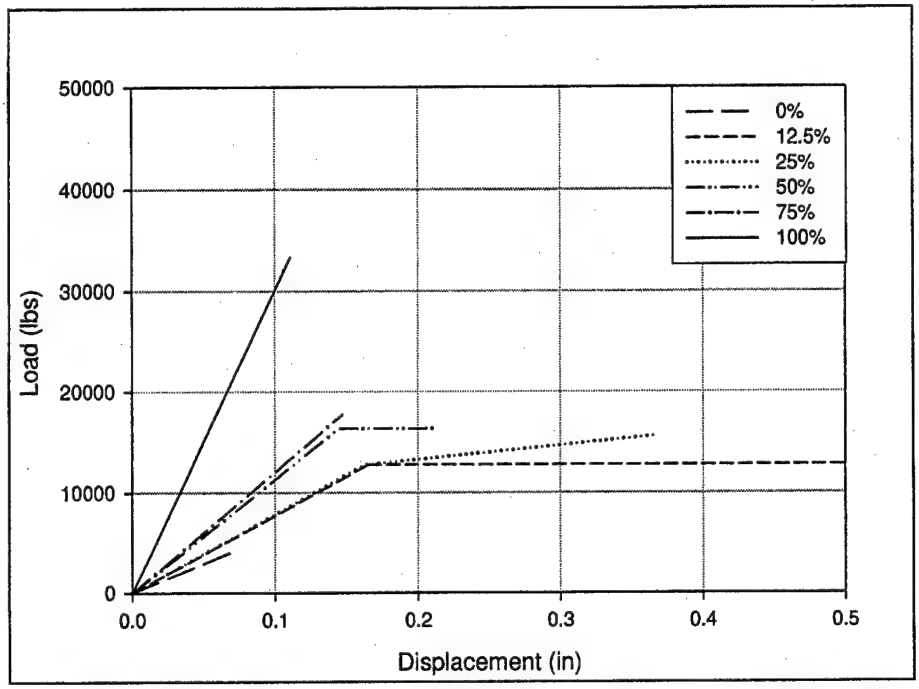

Figure 46. Idealized bilinear curve fit for Series I from 0% through 100% normal load.

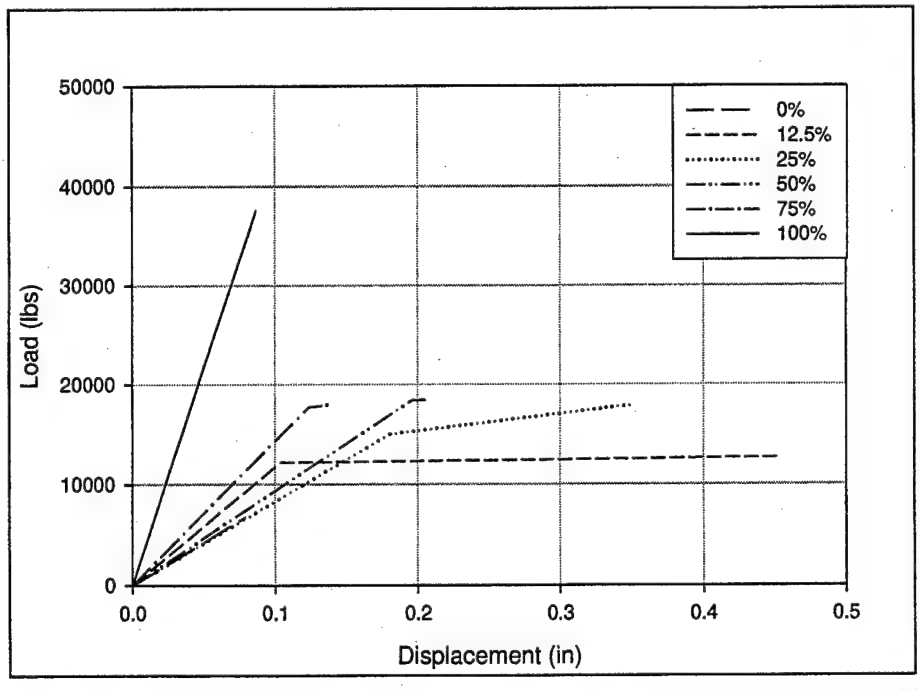

Figure 47. Idealized bilinear curve fit for series II from 0% through 100% normal load.

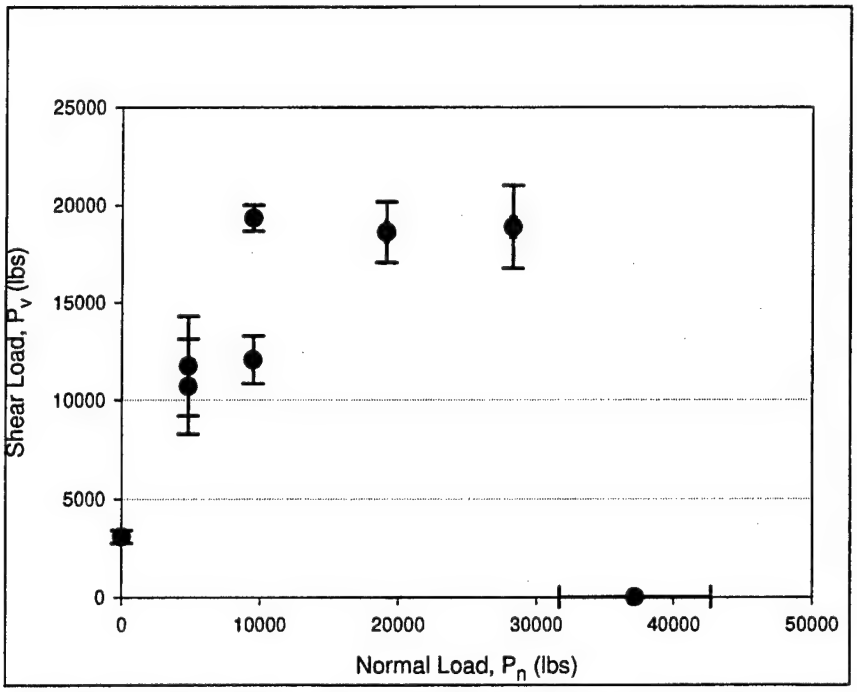

Figure 48. Normal load vs shear load (yield and ultimate) for Series 0.

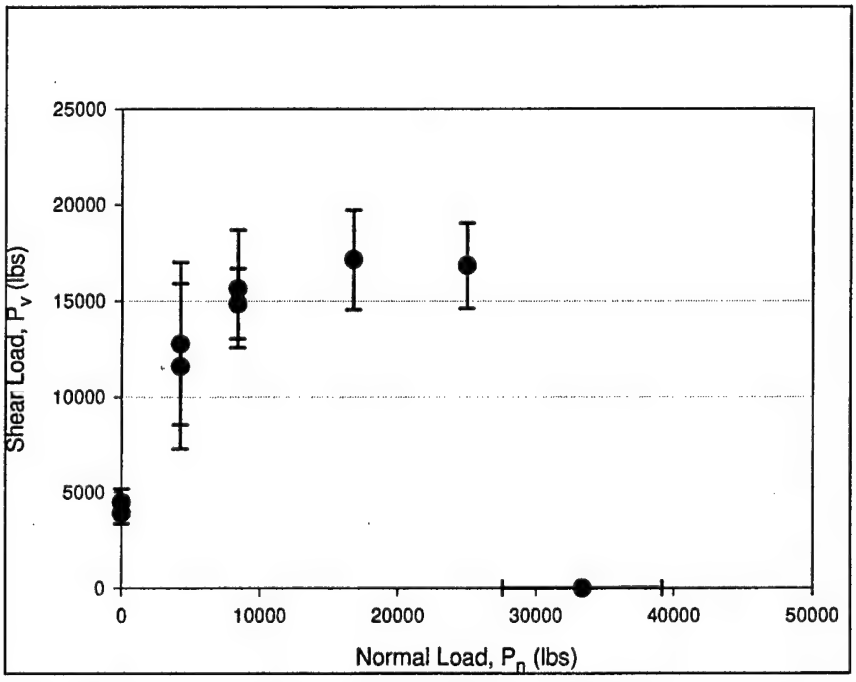

Figure 49. Normal load vs shear load (yield and ultimate) for Series I.

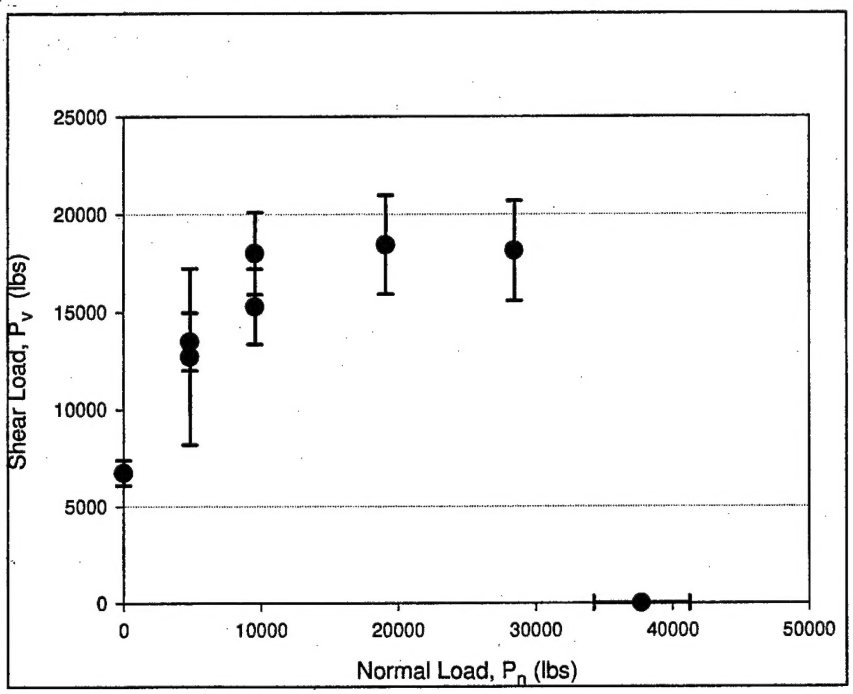

Figure 50. Normal load vs shear load (yield and ultimate) for Series II.

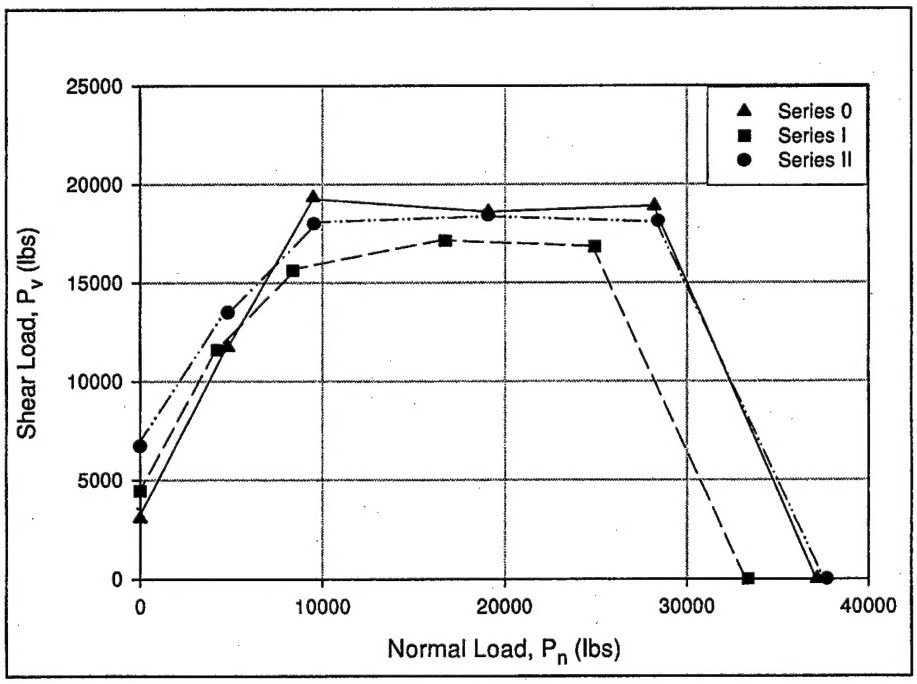

Figure 51. Absolute normal load vs shear load at ultimate for Series 0, I, and II.

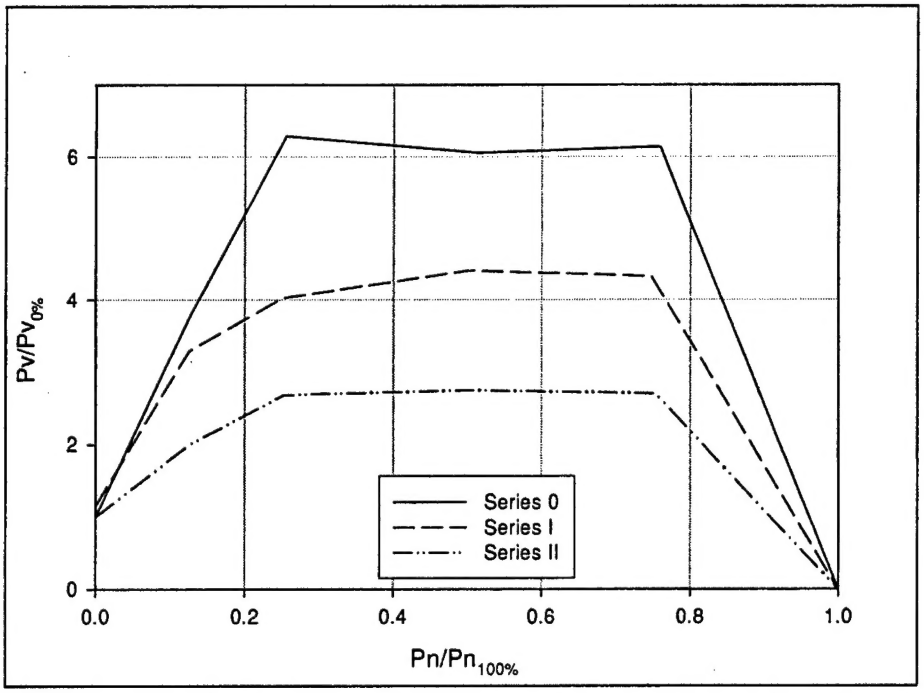

Figure 52. Normalized normal load vs shear load at ultimate for Series 0, I, and II.

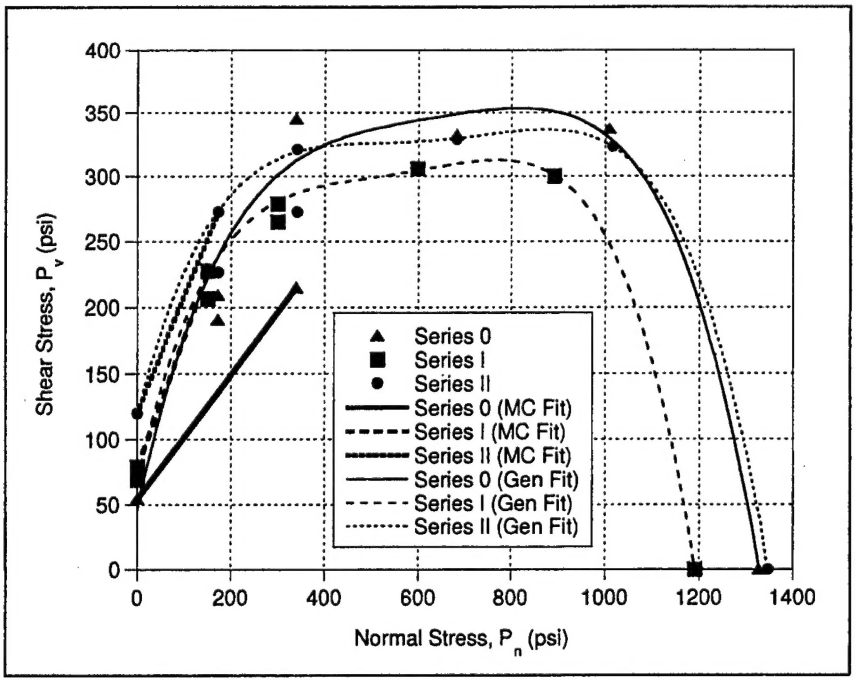

Figure 53. Normal stress vs shear stress with Mohr-Coulomb and Generalized Failure Criteria.

CERL Distribution

Chief of Engineers
ATTN: CEHEC-IM-LH (2)

Engineer Research and Development Center (Libraries)
ATTN: ERDC, Vicksburg, MS
ATTN: Cold Regions Research, Hanover, NH
ATTN: Topographic Engineering Center, Alexandria, VA

Defense Tech Info Center 22304
ATTN: DTIC-O

5
9/02

REPORT DOCUMENTATION PAGE

Form Approved
OMB No. 0704-0188

Public reporting burden for this collection of information is estimated to average 1 hour per response, including the time for reviewing instructions, searching existing data sources, gathering and maintaining the data needed, and completing and reviewing this collection of information. Send comments regarding this burden estimate or any other aspect of this collection of information, including suggestions for reducing this burden to Department of Defense, Washington Headquarters Services, Directorate for Information Operations and Reports (0704-0188), 1215 Jefferson Davis Highway, Suite 1204, Arlington, VA 22202-4302. Respondents should be aware that notwithstanding any other provision of law, no person shall be subject to any penalty for failing to comply with a collection of information if it does not display a currently valid OMB control number. PLEASE DO NOT RETURN YOUR FORM TO THE ABOVE ADDRESS.

1. REPORT DATE (DD-MM-YYYY)	2. REPORT TYPE	3. DATES COVERED (From - To)
12-2002	Final	

4. TITLE AND SUBTITLE
Biaxial Loading and Failure Behavior of Brick Triplets with Fiber-Reinforced Polymer Composite Upgrades

5a. CONTRACT NUMBER

5b. GRANT NUMBER

5c. PROGRAM ELEMENT NUMBER

6. AUTHOR(S)
J.B. Berman, G.K. Al-Chaar, and P.K. Dutta

5d. PROJECT NUMBER
40162784AT41

5e. TASK NUMBER

5f. WORK UNIT NUMBER
CFM-A081

7. PERFORMING ORGANIZATION NAME(S) AND ADDRESS(ES)
U.S. Army Engineer Research and Development Center (ERDC) Construction Engineering Research Laboratory (CERL) P.O. Box 9005
Champaign, IL 61826-9005

8. PERFORMING ORGANIZATION REPORT NUMBER
ERDC TR-02-7

9. SPONSORING / MONITORING AGENCY NAME(S) AND ADDRESS(ES)
HQ USACE
441 G Street
Washington, DC 20314-1000

10. SPONSOR/MONITOR'S ACRONYM(S)
CECW-EW

11. SPONSOR/MONITOR'S REPORT NUMBER(S)

12. DISTRIBUTION / AVAILABILITY STATEMENT
Approved for public release; distribution is unlimited.

13. SUPPLEMENTARY NOTES
Copies are available from the National Technical Information Service, 5285 Port Royal Road, Springfield, VA 22161.

14. ABSTRACT

To facilitate both engineering research and the design of unreinforced masonry (URM) structures, a standardized procedure for testing small-scale brick panel specimens would be beneficial. Some researchers have conducted simple monoaxial shear tests on brick triplet specimens, but these have tended to be unrealistic because they do not account for the effects of normal gravity loads. However, a triplet test that properly accounts for normal loading effects could be as useful to the construction industry as standard concrete cylinder and mortar cube tests. In support of a larger study on URM seismic rehabilitation techniques, the authors developed a triplet shear test that accounts for normal loads.

One hundred brick triplets were tested. About one-third were strengthened on one side with fiber-reinforced polymer (FRP) material, and another third were strengthened on two sides. The remaining triplets were not reinforced. Each type of triplet was shear-tested to failure under one of six different percentages of ultimate normal capacity. The results were analyzed, compared and incorporated into the results of the larger study. It is concluded that the triplet test can provide a useful estimate of the shear capacity and failure modes of masonry wall systems in the field.

15. SUBJECT TERMS
Fiber reinforced polymer (FRP), composite materials, structural engineering, masonry, seismic testing

16. SECURITY CLASSIFICATION OF:			17. LIMITATION OF ABSTRACT	18. NUMBER OF PAGES	19a. NAME OF RESPONSIBLE PERSON
a. REPORT	b. ABSTRACT	c. THIS PAGE			Ghassan K. Al-Chaar
Unclassified	Unclassified	Unclassified	SAR	62	19b. TELEPHONE NUMBER (Include area code) 217-352-6511